Green Chemistry

PAPER

Cite this: *Green Chem.*, 2023, **25**, 5878

Insights into the reaction network and kinetics of xylose conversion over combined Lewis/Brønsted acid catalysts in a flow microreactor†

Wenze Guo, [a,b] Herman Carolus Bruining,[a] Hero Jan Heeres [a] and Jun Yue *[a]

The catalytic effect of Lewis acid on xylose conversion to furfural has been widely reported, while the underlying reaction network and kinetics are not fully elucidated. This work presents experimental and kinetic modelling studies on xylose conversion to furfural, using $AlCl_3$/HCl as combined Lewis/Brønsted acid catalysts in monophasic water or a biphasic water–methyl isobutyl ketone system in a flow microreactor. The reaction network and kinetics were developed, where $Al(OH)_2^+$ was identified as the catalytically active species for isomerization between xylose, lyxose and xylulose, while both $Al(OH)_2^+$ and H^+ catalyze the sugar dehydration to furfural and side reactions leading to humins (*e.g.*, sugar condensation and furfural degradation). The promoting effect of $AlCl_3$ is attributed to not only the tandem catalysis through xylulose, but also the parallel $Al(OH)_2^+$-catalyzed sugar dehydration. Within the studied range (120 to 180 °C, 0.05–0.4 M HCl, 0.04–0.12 M $AlCl_3$), the furfural selectivity relied mainly on the concentration ratio of HCl to $AlCl_3$ rather than their individual concentrations or the temperature. The volcano-like evolution of the maximum furfural yield with increasing HCl/$AlCl_3$ ratio is related to (i) the lower reaction orders in $Al(OH)_2^+$ for reactions forming furfural than for side reactions; and (ii) a gradual shift of the dominant reaction pathway from the $Al(OH)_2^+$-catalyzed one towards H^+-catalyzed one. An optimized furfural yield up to 90% was achieved with 40 mM $AlCl_3$ and 100 mM HCl at 160 °C from 1 M xylose in a continuous slug flow microreactor. The catalytic aqueous phase could be recycled and reused four times without performance loss.

Received 13th January 2023,
Accepted 4th April 2023

DOI: 10.1039/d3gc00153a

rsc.li/greenchem

1. Introduction

Worldwide industrial and economic development has led to a steady depletion of fossil reserves and significant CO_2 emission. To alleviate these environmental issues, significant research attention has been given to utilizing lignocellulosic biomass, which is composed mainly of cellulose, hemicellulose and lignin, as a green and sustainable alternative feedstock for the production of fuels, materials and chemicals.[1,2] In a biomass valorization network, one representative pathway is the conversion of lignocellulosic carbohydrates to bio-based furanic platform chemicals.[3,4] One such carbohydrate is xylose, the most abundant pentose in the hemicellulose fraction (25–35% on a dry basis).[5] Dehydration of xylose produces furfural, a versatile building block for the production of a spectrum of biofuels, biobased polymers and chemicals.[6] For example, the hydrogenation of furfural produces furfuryl alcohol as the monomer of furan resins,[7] 2-methylfuran and 2-methyltetrahydrofuran as potential liquid transportation fuel additives,[2,8,9] and tetrahydrofuran as a widely used industrial specialty solvent.[10] Moreover, furfural can be transformed *via* a series of aldol condensation and dehydration/hydrogenation reactions to liquid alkanes that serve as gasoline, diesel or aviation fuel.[11]

Typically, furfural is produced by xylose dehydration in water under the catalysis of homogeneous Brønsted acids such as HCl, H_2SO_4 and H_3PO_4, which involves the dehydration of xylose to furfural and a series of undesirable side reactions leading to humins, such as xylose condensation and furfural degradation.[12] Furfural production from biomass has a long history of over 100 years (dating back to 1921 by the Quaker Oats Company[13]) and currently is still conducted in energy-intensive processes using high-pressure steam to supply heat and strip out furfural in batch or continuous reactors over homogeneous acid catalysts, which gives limited furfural

[a]*Department of Chemical Engineering, Engineering and Technology Institute Groningen, University of Groningen, Nijenborgh 4, 9747 AG Groningen, The Netherlands. E-mail: yue.jun@rug.nl*
[b]*State Key Laboratory of Chemical Engineering, Department of Chemical Engineering, East China University of Science and Technology, Shanghai 200237, PR China*

† Electronic supplementary information (ESI) available. See DOI: https://doi.org/10.1039/d3gc00153a

yields of only *ca.* 50% due to the severe carbon loss to humins.[14] Heterogeneous catalysis is usually preferred due to the ease of catalyst separation and reuse, and solid acid catalysts have received significant attention for the synthesis of furanics from C5/C6 sugars.[14–18] However, issues still need to be addressed such as the poor hydrothermal stability of solid acid catalysts, long reaction time (>1 h), and need for frequent regeneration due to the humin deposition.[14,15] Consequently, a green and efficient homogeneous catalytic system and process is still attractive for (scaled-up) furfural production.

One typical strategy to improve the furfural yield is suppressing the furfural degradation by its *in situ* extraction from the aqueous reaction media using an organic phase (*i.e.*, biphasic solvent system). It is well known that batch reactors for reactions in biphasic systems usually suffer from poor flow pattern control and mixing when scaled up, and as such the low heat/mass transfer efficiency therein tends to limit the xylose conversion and furfural yield. Recently, continuous flow processing in microreactors has been used as a promising tool for fast kinetic studies and an efficient production platform for the synthesis of furanics such as 5-hydroxymethylfurfural (HMF) or 5-chloromethylfurfural (CMF) from C6 sugars in monophasic or biphasic solvent systems,[18–26] due to advantages such as the superior heat/mass transfer rates, precise process control and ease of productivity increase.[27,28] Comparatively, there have been fewer reports about the application of microreactors for furfural synthesis. We have recently reported the use of a slug flow microreactor for xylose conversion over an HCl catalyst in a water (with 10 wt% NaCl addition)–methyl isobutyl ketone biphasic system, where a promising furfural yield up to 93% was achieved at 180 °C and 4 min.[29] The furfural extraction rate was estimated to be two orders of magnitude higher than the rate of furfural formation or degradation, rendering the reaction under kinetic control.

Besides furfural degradation, which can be mitigated by efficient extraction, xylose condensation is the other cause of the carbon loss to humins. Therefore, another strategy to boost the furfural yield is to regulate the xylose reaction network to reduce its condensation. Our recent work demonstrated the use of chloride ions to improve the xylose reaction kinetics by promoting the xylose dehydration and suppressing its condensation.[29] Beyond the high furfural yield (93% from 1 M xylose), the addition of 10 wt% NaCl in the aqueous phase somewhat increased the viscosity and imposed additional operation difficulty for the microreactor system. Therefore, in this work we have explored another possibility to improve the xylose conversion chemistry. It has been reported that xylulose, an isomer of xylose, gives by far higher kinetic rates and furfural yields compared with xylose.[30] In the past years, several mineral Lewis acids such as Cr(III), Fe(III) and Al(III) have been reported to be active for xylose isomerization to xylulose in water.[30–33] This opens the opportunity for a concept of tandem catalysis where xylose is isomerized *in situ* to xylulose (over a Lewis acid) followed by xylulose dehydration to furfural (over a Brønsted acid) in high yields. Among others, Cr(III) is toxic and carcinogenic, and Fe(III) is highly active for the side reactions leading to humins,[31] while Al(III) (*e.g.* $AlCl_3$) is cheap with low toxicity. Yang *et al.*[32] reported a furfural yield of 75% from xylose in a NaCl–water/tetrahydrofuran biphasic system using $AlCl_3$ as the catalyst at 140 °C in a microwave-heated batch reactor. Yang *et al.*[33] reported a furfural yield of up to 87.8% from xylan using $Al_2(SO_4)_3$ as the catalyst under microwave conditions, and the hexa-coordinated $Al(OH)_2^+$ species were suggested to be the active sites for xylose–xylulose isomerization *via* ESI-MS spectrometry. However, in both cases, Al(III) was used solely without the addition of an external Brønsted acid, which might deviate from the optimal scenario for tandem acid catalysis. It is known that Al(III) hydrolyzes rapidly in water to form various species such as $[Al(H_2O)_6]^{3+}$, $[Al(OH)(H_2O)_5]^{2+}$ and $[Al(OH)_2(H_2O)_4]^+$, *etc.*, depending on the pH value, initial Al(III) concentration and temperature. Considering that Lewis and Brønsted acids catalyze different reactions, and the amount of Lewis acidic Al species is regulated by Brønsted acidity *via* a hydrolysis equilibrium (eqn (S1)–(S4)†), it is important to investigate the interaction between the two acid types and the relevant effects on the sub-reactions within the xylose conversion network. Mittal *et al.*[34] briefly reported furfural synthesis from hemicellulose (present in untreated poplar wood) over a combination of 33 mM HCl and 8 mM $AlCl_3$ in a monophasic dioxane/water (4 : 1) solvent system, where a promising furfural yield of 91% was obtained at 200 °C in 5 min. Lopes *et al.*[31] investigated the catalytic effect of $CrCl_3$, $FeCl_3$ and $AlCl_3$ combined with formic acid as the catalyst for xylose conversion in monophasic water, and the best result was found with $AlCl_3$, giving a furfural yield of *ca.* 70% at 130 °C. An empirical kinetic model was developed; however, it lacks insights into the catalytically active Al species and their amount variation with Brønsted acidity, which limits the model's use for other conditions. In general, despite the promising furfural yields over the $AlCl_3$ catalyst as reported in the literature, deep knowledge is still required on aspects such as (i) the xylose conversion network and the role of Lewis and Brønsted acids therein; (ii) the catalytically active Al species responsible for the sub-reactions within the xylose conversion network; (iii) the interaction between the Lewis acid ($AlCl_3$) and Brønsted acid (HCl), and their regulating effects on xylose conversion; and (iv) a comprehensive kinetic model with the quantitative incorporation of catalytically active Al species under varying reaction conditions. Such a model has not been reported so far, but is of great importance for a proper process design and optimization for efficient furfural production from xylose *via* synergetic Lewis/Brønsted acid catalysis, and thus is one of the aims in this work.

Herein, experiments on xylose (as well as lyxose, xylulose and furfural) using $AlCl_3$ or (and) HCl as the catalyst were firstly performed in monophasic water in a flow microreactor to study the kinetics under varying conditions (temperature of 120 to 180 °C, HCl concentration of 0.05 to 0.4 M, $AlCl_3$ concentration of 0.04 to 0.12 M, and each substrate concentration of 0.01 to 0.5 M). Based on the reaction results, the xylose conversion network was developed and the role of Lewis and Brønsted acids therein was elucidated. Advanced mass spec-

troscopy on model reactants was performed to identify the catalytically active Al species and study its variation with varying $AlCl_3$/HCl ratios. The amounts of active Al species were quantified according to the hydrolysis equilibrium of $AlCl_3$ and incorporated into the kinetic model, which consists of a separate Brønsted acid-catalyzed part and a Lewis acid-catalyzed part. Kinetic parameters for the conversion of individual sugars and furfural over Al species or H^+ were estimated by fitting the model to the experimental data. Furthermore, xylose conversion using the combined $AlCl_3$/HCl catalyst was performed in a water–methyl isobutyl ketone (MIBK; inexpensive, low toxicity and high furfural partition capacity) biphasic system in a slug flow microreactor, where the results were shown to be well described by the kinetic model with the incorporation of furfural extraction between the phases. Process optimization for the furfural yield was conducted based on the kinetic model. Moreover, the recyclability and reusability of the homogeneous catalyst were also demonstrated, and a performance comparison with literature work was made to highlight the potential of the present process using microreactors for the efficient furfural synthesis from xylose.

2. Methods

2.1 Materials

D-Xylose (99 wt%), D-lyxose (99 wt%), aluminum chloride hexahydrate (99 wt%), and hydrochloric acid (37 wt%) were all purchased from Sigma-Aldrich Co., Ltd. MIBK (99 wt%) was purchased from Acros Organics Co., Ltd. D-Xylulose was purchased from Carbosynth, UK. All chemicals were of chemical grade and used as received without any further treatment. Milli-Q water was used to prepare solutions throughout all the experiments. Perfluoroalkoxy alkane (PFA) tubing (inner diameter: 1.65 mm) was supplied by the Swagelok company and used as capillary microreactors.

2.2 Experimental setup and procedure

Experiments on the conversion of sugars or furfural using HCl and (or) $AlCl_3$ as the catalyst were conducted in the microreactor in monophasic water or biphasic water–MIBK solvent systems. Monophasic experiments were performed to study the xylose conversion network and the role of HCl and $AlCl_3$ under a wide range of conditions, including a temperature range from 120 to 180 °C, initial concentration of substrates (xylose, xylulose, lyxose and furfural) between 0.01 and 0.5 M, HCl concentration of 0.05 to 0.4 M, and $AlCl_3$ concentration of 0.04 to 0.12 M (*cf.* more details in Table S1†). Biphasic experiments were performed under some representative conditions mentioned above in a slug flow microreactor, with an initial organic to aqueous volumetric flow ratio (O/A) of 1 to 4 (fed at 20 °C).

Fig. 1a shows the slug flow microreactor setup used for xylose conversion to furfural. The setup and procedure are similar to that reported in our previous work.[19,20,29] Typically, the aqueous feed contained sugars or furfural as well as HCl and (or) $AlCl_3$ catalyst, and the organic feed was MIBK. Both phases were fed to the microreactor using a binary HPLC pump unit (Agilent 1200 Series). A uniform slug flow was generated in the downstream PFA capillary microreactor by mixing two phases in a polyether ether ketone (PEEK) Y-connector (inner diameter: 1.65 mm; Fig. 1b). The hydrophobic nature of the PFA microreactor renders MIBK as the continuous phase, and the aqueous reaction phase as droplets which are not in direct contact with the microreactor to avoid humin deposition on the wall causing blockage.[19,20,29] The microreactor was coiled around an aluminum block in an oven maintained at a certain temperature. The reaction was quenched by a water bath (*ca.* 20 °C) at the microreactor exit. The pressure in the

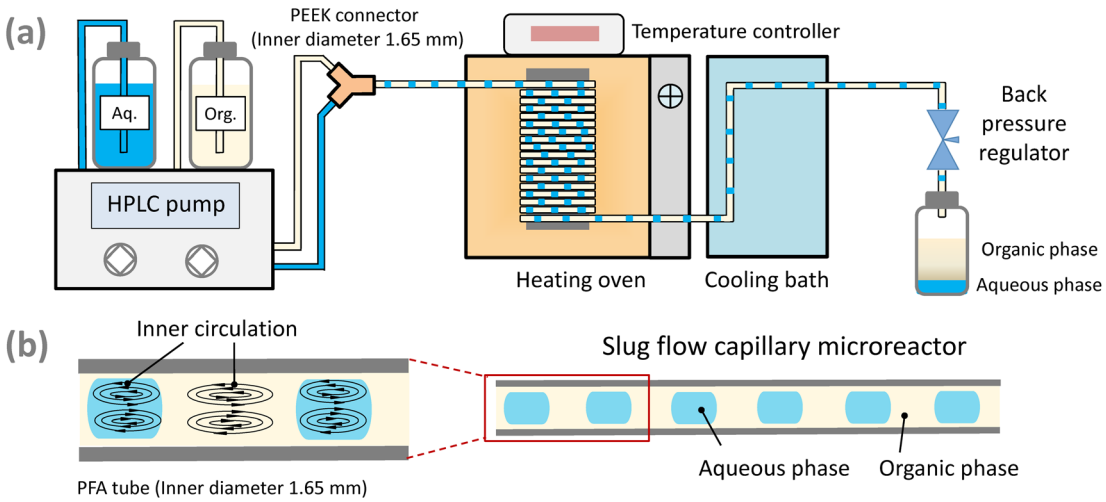

Fig. 1 (a) Schematic diagram of the slug flow microreactor system for continuous furfural synthesis from xylose. (b) The slug flow consisted of aqueous droplets and organic slugs, where the inner circulation promoted mixing/reaction in the aqueous phase and enhanced furfural extraction to the organic phase.

microreactor was maintained at *ca.* 10 bar by a back-pressure regulator at the end of the microreactor to maintain the reactor content in the liquid state. Product samples were collected after the system reached steady state (*i.e.*, after *ca.* 4 times the residence time in the microreactor). The length of the microreactor (L), *i.e.*, the section inside the oven, is typically 3.3 m. For experiments aimed at investigating the mass transfer limitation, microreactors of 1.2 m and 16.9 m length were also used. The residence time (τ) in the microreactor was varied by adjusting the flow rates (details about the calculation of τ and the actual flow rates have been previously reported[19]). The collected aqueous and organic phases were filtered through a polytetrafluoroethylene (PTFE, 0.45 μm) filter, and subsequently analyzed by high performance liquid chromatography (HPLC) and gas chromatography (GC), respectively.

Monophasic kinetic experiments were performed in the same setup as above with the organic-phase flow being stopped. Before each run, the microreactor was flushed with water to remove any possibly remained humins.

The above monophasic and biphasic experiments under representative conditions were conducted at least twice, the results of which are reproducible within a 5% standard deviation.

2.3 Analysis and characterization

The composition of the aqueous phase was analyzed by an Agilent 1200 HPLC, equipped with an Agilent 1200 pump, a refractive index detector, a standard ultraviolet detector as well as a Bio-Rad organic acid column (Aminex HPX-87H). A diluted aqueous H_2SO_4 solution (5 mM, 0.55 mL min^{-1}) was used as the eluent, and the temperature of the column was maintained at 60 °C. A difficulty in the analysis is in the quantification of xylulose and lyxose due to their similar retention times on the HPLC chromatogram leading to severe overlapping[30,31] (12.9 min for xylulose and 13.1 min for lyxose in this work; *cf.* Fig. S1a†), which may be the reason that some earlier studies have not reported lyxose as a xylose isomerization product.[32,33] In this work, this issue was addressed using a Gaussian deconvolution method for data treatment,[31] where the peak areas of xylulose and lyxose were obtained by deconvoluting their overlapped curve (Fig. S1b; the details are discussed in section S2 in the ESI†). The organic phase was analyzed by TraceGC Ultra GC, equipped with a flame ionization detector and a fused silica column (Stabilwax-DA). The concentrations of the components in the aqueous and organic samples were determined from the calibration curves obtained using the standard solutions with known compounds and concentrations.

Electro-spray ionization mass spectra (ESI-MS) were recorded on an Orbitrap XL mass spectrometer (Thermo Fisher Scientific) with ESI ionization in the positive mode. Solution samples of xylose, lyxose, xylulose and furfural containing $AlCl_3$ and HCl were measured in the range of m/z 100–600 in positive mode. The data acquisition and analyses were performed on Xcalibur software.

2.4 Definitions and calculations

The conversion of substrate i (X_i) and the yield of product j (Y_j) are defined by

$$X_s = \frac{Q_{aq,0}C_{aq,s,0} - Q_{aq,1}C_{aq,s,1}}{Q_{aq,0}C_{aq,s,0}} \times 100\% \quad (1)$$

$$Y_p = \frac{Q_{org,1}C_{org,p,1} + Q_{aq,1}C_{aq,p,1}}{Q_{aq,0}C_{aq,s,0}} \times 100\% \quad (2)$$

where Q_{aq} and Q_{org} represent the flow rates of the aqueous and organic phases, respectively. C_{aq} and C_{org} are the concentrations in the aqueous and organic phases, respectively. The subscripts 0 and 1 refer to the start of the reaction at the microreactor inlet (*i.e.*, at *ca.* 20 °C) and the end of the reaction at the microreactor outlet (*i.e.*, after being cooled to *ca.* 20 °C), respectively. Due to the partial miscibility between MIBK and water, $Q_{aq,1}$ and $Q_{org,1}$ differ from $Q_{aq,0}$ and $Q_{org,0}$, respectively, and were corrected as

$$Q_{aq,1} = Q_{aq,0}\gamma_{aq} \quad (3)$$

$$Q_{org,1} = Q_{org,0}\gamma_{org} \quad (4)$$

where γ_{aq} or γ_{org} is the correction factor which represents the ratio of the volumetric flow rates at the microreactor outlet and inlet (both at *ca.* 20 °C) for either the aqueous or organic phase, respectively. The values of γ_{aq} and γ_{org} are estimated using Aspen Plus simulation[19] and listed in Table S2† for some given initial MIBK to water volumetric flow ratios.

The carbon balance is defined by

$$C \text{ balance} = \frac{C \text{ amount in the products} + C \text{ amount in the remaining substrate}}{C \text{ amount in the starting substrate}} \times 100\% \quad (5)$$

The carbon balance is based on the quantified known products by HPLC and GC (xylose, xylulose, lyxose and furfural). It does not account for the non-identified soluble/insoluble byproducts.

The amount of aluminum species and H^+ in water under varying temperatures and initial concentrations of $AlCl_3$ and HCl is calculated according to the hydrolysis equilibrium of $AlCl_3$ in water. The calculation procedure and the results under some representative conditions are provided in sections S4, S8 and Table S5 of the ESI.†

3. Results and discussion

3.1 Furfural synthesis from xylose using HCl or combined HCl/$AlCl_3$ as the catalyst in a biphasic slug flow microreactor

We first demonstrated xylose conversion using HCl with or without the addition of $AlCl_3$ as the catalyst at 160 °C in the water/MIBK biphasic system in slug flow microreactors. In a typical run over the individual HCl (200 mM) catalyst, the furfural yield increased gradually to a maximum of 79% at 25 min with a xylose conversion of 97%. In the meantime, the

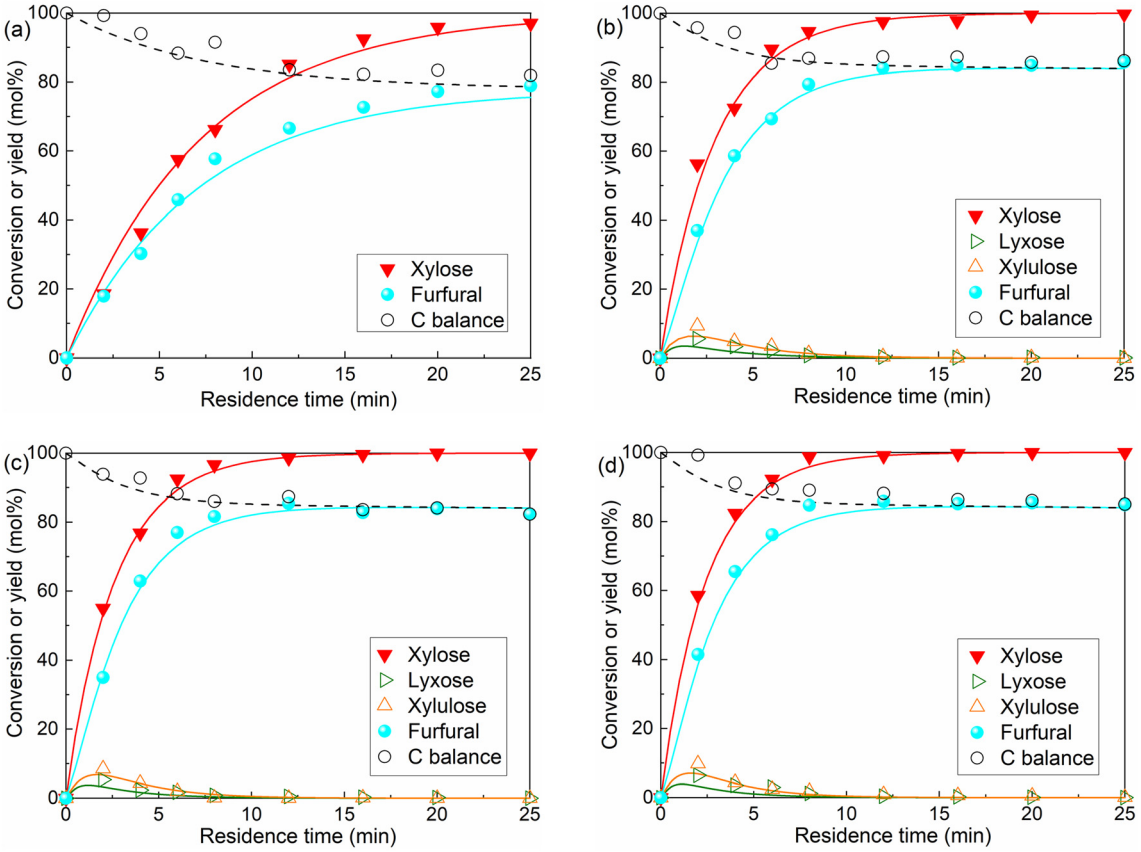

Fig. 2 Furfural synthesis from xylose in a biphasic slug flow microreactor over (a) 200 mM HCl, (b) 200 mM HCl and 40 mM $AlCl_3$, (c) 200 mM HCl and 80 mM $AlCl_3$, and (d) 200 mM HCl and 120 mM $AlCl_3$. Reaction conditions: 160 °C, 0.1 M xylose, L = 3.3 m, O/A = 4. Symbols denote the experimental data and lines are the model values (the same in Fig. 3, 7–9 and 14 shown hereafter).

carbon balance decreased gradually to less than 80%, due to the carbon loss to humins *via* xylose condensation and furfural degradation (Fig. 2a). After the addition of 40 mM $AlCl_3$, xylulose and lyxose appeared as the respect isomerization and epimerization products of xylose, the yields of which showed clear maxima at an early stage of the reaction, indicating that these are intermediate products which were fast prone to further chemistry (Fig. 2b). Moreover, a far higher xylose conversion rate, as well as a higher furfural yield, were observed in comparison with the case catalyzed by solely HCl (Fig. 2a). The furfural yield reached 86% at 16 min and then stayed stable with a prolonged residence time to 25 min. The improved carbon balance, which remained over 85%, suggests a reduced overall humin formation (Fig. 2b). A similar promoting effect of $AlCl_3$ was also observed with the addition of 80 mM $AlCl_3$ and 120 mM $AlCl_3$, and no distinct differences in the xylose conversion and product yields were observed among these different $AlCl_3$ loadings under the current reaction conditions (Fig. 2b–d). Besides $AlCl_3$, other Lewis acids such as $CrCl_3$ and $FeCl_3$ have also been reported to improve the furfural yield, and most researchers attributed this to the tandem catalysis comprising xylose isomerization to xylulose followed by xylulose dehydration to furfural in higher yields.[30–33] To compare the reaction performance of xylose with its isomers, benchmark experiments with xylulose and lyxose as the substrate were performed under otherwise the same conditions (160 °C, 200 mM HCl) (Fig. S2†). Indeed, a higher conversion rate was observed for xylulose and lyxose (Fig. S2a†). However, despite the higher furfural yield obtained from xylulose, the maximum furfural yield is only *ca.* 82%, which is lower than that (*ca.* 86%) in the present work using combined HCl/$AlCl_3$ as the catalyst, not to mention the lower maximum furfural yield (*ca.* 74%) given by lyxose, the other isomer of xylose (Fig. S2b†). Therefore, we believe that the tandem catalysis *via* xylulose at least should not be the only reason for the promoting effect of Lewis acid $AlCl_3$. To reveal more fine details for a deeper process understanding and optimization, clear insights into the xylose reaction network, the role of HCl and $AlCl_3$ therein, and the reaction kinetics are of great importance and will be addressed hereafter (*vide infra*).

3.2 Xylose conversion network and the role of Lewis and Brønsted acids: monophasic experiments with sugars or furfural using $AlCl_3$ or HCl as the catalyst in the microreactor

Since $AlCl_3$ hydrolyzes in water to form various aluminum species and H^+ (*cf.* eqn (S1)–(S6)†), the catalytic effect of $AlCl_3$

may be related to all of them. To understand the role of Lewis acid (Al species from $AlCl_3$) and Brønsted acid (H^+) catalysts in the reaction (*e.g.*, glucose conversion), some researchers conducted comparative reactions over individual $AlCl_3$ or HCl while maintaining the pH for both cases identical at room temperature.[35] However, this might not be precise as the hydrolysis equilibrium of $AlCl_3$ in water is a strong function of temperature (eqn (S6)†), and thus the actual H^+ concentration in $AlCl_3$ solution at the reaction temperature differs significantly from that at room temperature. For example, the H^+ concentration in 40 mM $AlCl_3$ solution was calculated to increase from 0.39 mM at 20 °C to 19 mM at 160 °C (Table S5†). Therefore, to understand the xylose conversion network and precisely distinguish the impact of Lewis and Brønsted acids, herein monophasic experiments with xylose and its reaction intermediates (furfural, lyxose and xylulose) were comparatively investigated under the catalysis of either $AlCl_3$ (40 mM) or HCl (21.1 mM) with equal Brønsted acidity (19.0 mM H^+) at 160 °C.

3.2.1 Experiments with furfural. When using furfural as the substrate and $AlCl_3$ as the catalyst, the conversion of furfural is 83.5% at a residence time of 25 min (Fig. 3a), which is by far higher than in the reaction with HCl only (4.3%; Fig. 3b). This implies that Al species, in addition to H^+, catalyze the furfural degradation. The carbon balance in both cases became worse with increasing furfural conversion, owing to the more significant formation of unidentified products (*e.g.*, oligomers or humins).

3.2.2 Experiments with lyxose. When starting from lyxose in the presence of $AlCl_3$, the lyxose conversion increased rapidly and reached over 99% within 8 min (Fig. 3c). Simultaneously, the furfural yield decreased steadily from a maximum of 64.7% at 2 min to 21.3% at 25 min, due to the severe furfural degradation to, among others, humins catalyzed by both Al species and H^+ (Fig. 3a and b). Xylose and xylulose were observed in small amounts at an early stage of the reaction, the respective yields reaching maxima of 3.5% and 0.9% at 2 min, while in the presence of only HCl (Fig. 3d), no such isomer products were detected. This indicates that the reversible epimerization between lyxose and xylose, as well as the following isomerization between xylose and xylulose (and possibly the isomerization between lyxose and xylulose), is only catalyzed by Lewis acid (Al species). Besides, the HCl-catalyzed lyxose conversion and furfural yield (being 67.4% and 47.4%, respectively, at 25 min and still on the rise), as well as the formation of unidentified products (mainly humins; *cf.* carbon balance), are by far lower than with $AlCl_3$ (Fig. 3c). One possible reason for the faster lyxose conversion and furfural formation in the latter case is that Al species promote the isomerization of lyxose to xylose and xylulose, and subsequently these isomer products are dehydrated to furfural and condensation to humins under the typical catalysis of HCl in a much higher rate than lyxose. However, control experiments using xylose, lyxose and xylulose as substrates, comparatively performed in the presence of 200 mM HCl at 160 °C, suggested an order in the conversion rate of lyxose > xylulose > xylose, and an order in the furfural yield of xylulose > lyxose > xylose (Fig. S2†). The even lower conversion rate of xylose and xylulose indicates that the HCl-catalyzed dehydration of these isomers is not the primary reason for the faster lyxose conversion. Based on this, another possibility, which tends to prevail, is that besides epimerization and isomerization, Al species directly catalyzes the conversion of lyxose and its isomers (xylose and xylulose) to furfural or humins. Additionally, it has been widely reported that Lewis acid promotes the polymerization of sugars such as xylose, fructose and glucose to

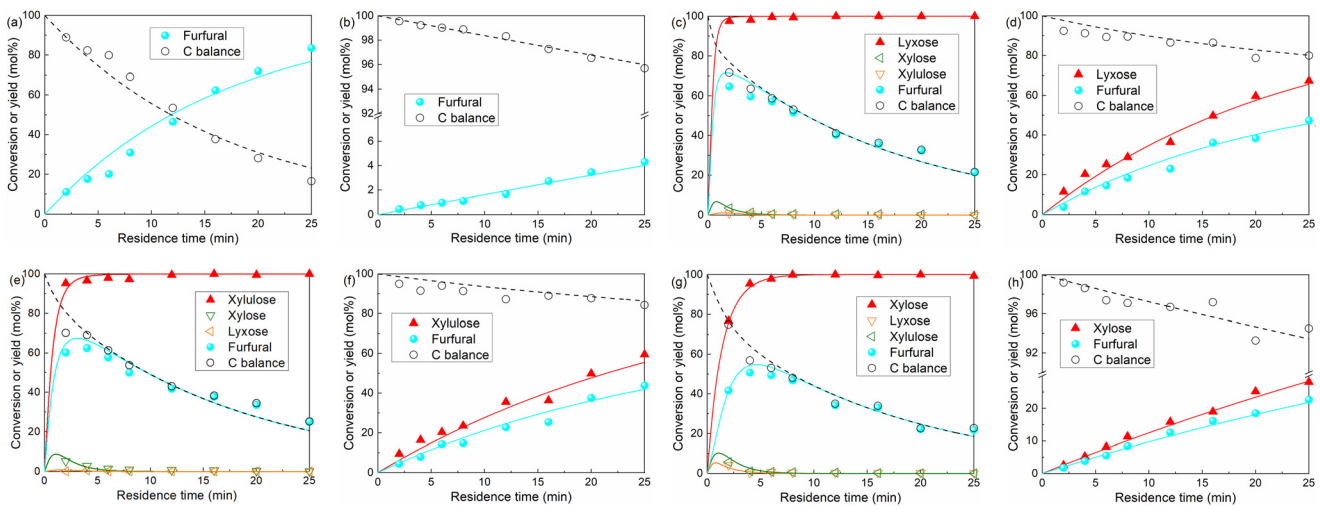

Fig. 3 Conversion of furfural and sugars using $AlCl_3$ or HCl as the catalyst in water in the microreactor: furfural conversion over (a) $AlCl_3$ and (b) HCl; lyxose conversion over (c) $AlCl_3$ and (d) HCl; xylulose conversion over (e) $AlCl_3$ and (f) HCl; xylose conversion over (g) $AlCl_3$ and (h) HCl. Reaction conditions: 0.1 M substrate, 160 °C, L = 3.3 m, 40 mM $AlCl_3$ or 21.1 mM HCl (both yielding the same Brønsted acidity, *i.e.*, 19.0 mM H^+, at 160 °C).

humins.[19,31] Therefore, the condensation of lyxose and its isomers to humins over Al species is also believed to contribute to the faster decrease of carbon balance in the presence of $AlCl_3$.

3.2.3 Experiments with xylulose. Experiments with xylulose as the substrate gave similar results compared with those with lyxose. In the presence of $AlCl_3$, small amounts of isomerization products such as xylose and lyxose were observed, the respective yields reaching 5.2% and 0.5% at 2 min, and these were then consumed rapidly to furfural or humins (Fig. 3e). Xylulose was fully converted within 6 min, and a maximum furfural yield of over 60% was obtained at 4 min (Fig. 3e). Comparatively, the reaction catalyzed by the individual HCl is much slower, as a xylulose conversion of 59.5% was obtained with a furfural yield of 43.8% at 25 min and was still on the rise (Fig. 3f). Similar to the case of lyxose, the by far faster xylulose conversion and furfural formation with $AlCl_3$ (than those with HCl) are attributed to the catalytic effect of both Al species and H^+ on the xylulose dehydration to furfural. In both cases, the carbon balance decreased as the reaction proceeded due to the sugar condensation and furfural degradation to unidentified products, which are catalyzed by both H^+ and Al species.

3.2.4 Experiments with xylose. For experiments with xylose in the presence of $AlCl_3$, xylose was fully converted within 8 min. Lyxose and xylulose (mainly derived from the epimerization and isomerization of xylose, respectively) were observed at a short residence time, the respective yields reaching 5.6% and 3.8% at 2 min (Fig. 3g). The minor amount of the isomer products (lyxose and xylulose; yields < 10%) from xylose is due to their fast dehydration to furfural and condensation to humins in the presence of $AlCl_3$ (Fig. 3c, e and g). The furfural yield reached a maximum of 50.7% at 4 min, followed by a steady decrease together with the decreasing carbon balance (Fig. 3g). In the presence of HCl, no lyxose and xylulose were detected, indicating the absence of isomerization reactions, and the xylose conversion and furfural yield are by far lower at the same residence time (Fig. 3h). As discussed in the experiments with lyxose and xylulose, the significantly faster xylose conversion, furfural formation and decrease of carbon balance over $AlCl_3$ are due to the additional catalytic effect of Al species.

3.2.5 Xylose conversion network and role of catalyst components. Based on the above experiments with furfural, lyxose, xylulose and xylose using either $AlCl_3$ or HCl as the catalyst (under the same Brønsted acidity at 160 °C), the xylose conversion network and the roles of Lewis acid and Brønsted acid therein are proposed (Fig. 4). In summary, the network involves the reversible isomerization and epimerization among xylose, xylulose and lyxose catalyzed only by Lewis acids (catalytically active Al species), the dehydration of these sugars to furfural and the degradation of sugars/furfural to among others humins (catalyzed by both Al species and H^+). Notably, here the parallel Lewis acid-catalyzed direct sugar dehydration to furfural (with higher rates than over H^+) is believed to also contribute to the promoting effect of Lewis acid on xylose conversion, in addition to the tandem catalysis *via* xylulose dehydration. Similar Lewis acid-catalyzed direct sugar dehydration has also been widely reported in the conversion of lignocellulosic carbohydrates to furfural or HMF (another bio-based platform chemical), over sole Lewis acid catalysts such as TiO_2, Nb_2O_5 and $Sc(OTf)_3$ without the presence of Brønsted acid (H^+).[18,19,35–39] However, the isolated Lewis acid is usually unselective towards furfural or HMF due to severe Lewis acid-catalyzed humin formation. Thus, its proper combination with additional Brønsted acids to regulate the reaction network is necessary for an optimized furfural synthesis (*vide infra*).

3.3 Insights into the catalytically active Al species for the sub-reactions within the xylose conversion network

In order to establish a comprehensive kinetic model that incorporates the interaction between Lewis and Brønsted acids and the corresponding impact on the xylose conversion under varying reaction conditions, it is important to determine the catalytically active Al species for the sub-reactions within the xylose conversion network. Lewis acidic metal ions such as Cr^{3+}, Fe^{3+} and Al^{3+} have been reported to catalyze the xylose conversion to furfural.[30–33] However, it is difficult to identify

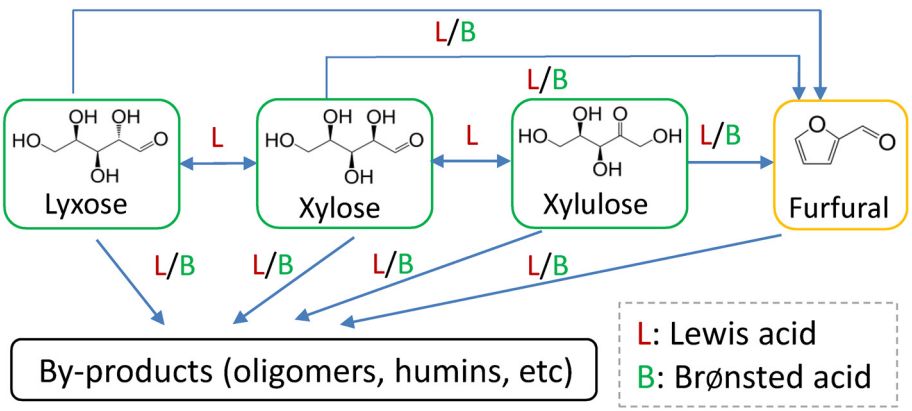

Fig. 4 The reaction network of xylose conversion in water and the role of Lewis and Brønsted acids in the sub-reactions.

their catalytically active species, due to the presence of a number of metal species that are in equilibrium with each other in water. For instance, $AlCl_3$ rapidly hydrolyzes in water to form various species such as $[Al(H_2O)_6]^{3+}$, $[Al(OH)(H_2O)_5]^{2+}$, $[Al(OH)_2(H_2O)_4]^{+}$ and $[Al(OH)_4]^{-}$, the amount of which depends on the initial $AlCl_3$ concentration, Brønsted acidity and temperature (*cf.* section S4 in the ESI†).[40] Yang *et al.*[33] observed xylose-coordinated $Al(OH)_2^{+}$ compounds in ESI-MS spectroscopy and suggested $Al(OH)_2^{+}$ as the active sites for xylose–xylulose isomerization using $Al_2(SO_4)_3$ as the catalyst in water. However, the coordination of Al species with other intermediates (lyxose, xylulose and furfural) within the xylose conversion network was not studied in their work and thus it lacks a comprehensive overview of the active Al species for different sub-reactions.

To gain insights into the active Al species for all the sub-reactions, herein aqueous $AlCl_3$/HCl solutions (40 mM $AlCl_3$ and 200 mM HCl) containing xylose, lyxose, xylulose or furfural were prepared and characterized by ESI-MS spectroscopy (Fig. 5). Peaks of [C5sugar + $Al(OH)_2$–$2H_2O$]$^+$, [C5sugar + $Al(OH)_2$–$3H_2O$]$^+$, [2C5sugar + $Al(OH)_2$–$2H_2O$]$^+$ and [2C5sugar + $Al(OH)_2$–$3H_2O$]$^+$ fragments (at m/z = 175.02, 157.01, 325.07 and 307.06, respectively) are present in the ESI-MS spectra of both the xylose and lyxose solutions (Fig. 5a and b). The spectrum of the xylulose solution also shows peaks at m/z = 157.01 and 175.02, corresponding to [xylulose + $Al(OH)_2$–$3H_2O$]$^+$ and [xylulose + $Al(OH)_2$–$2H_2O$]$^+$, respectively (Fig. 5c). Peaks from furfural-coordinated $Al(OH)_2^{+}$ compounds such as [furfural + $Al(OH)_2$]$^+$ and [furfural + $Al(OH)_2$ + $2H_2O$]$^+$ were also observed in the spectra of furfural solution at m/z = 157.01 and 193.03, respectively (Fig. 5d). The above-mentioned coordination compounds of $[Al(OH)_2]^+$ with xylose, lyxose, xylulose and furfural indicate that $[Al(OH)_2]^+$ is the main species that coordinates with xylose and its intermediates during the xylose conversion. Moreover, peaks corresponding to [Al + $(xylose)_n$]$^{3+}$, [Al(OH) + $(xylose)_n$]$^{2+}$ or [$Al(OH)_3$ + xylose + nH]$^{n+}$ species were not detected in the ESI-MS spectra of all samples. Therefore, [Al $(OH)_2$]$^+$ is believed to be the catalytically active Al species for the sub-reactions within the xylose reaction network.

An increase in the intensity of the peaks from xylose-coordinated $Al(OH)_2^{+}$ compounds was observed with increasing $AlCl_3$ loading (Fig. S3†), indicating that the amount of Al $(OH)_2^{+}$ as the catalytically active sites is a function of the relative Lewis/Brønsted acidity of the solution (*cf.* eqn (S1)–(S5)†). To provide more quantitative insights into the amounts of H^+ and $Al(OH)_2^{+}$ for kinetic studies, their concentrations under varying temperatures and initial concentrations of $AlCl_3$ and HCl were calculated and shown in Fig. 6. Generally, the

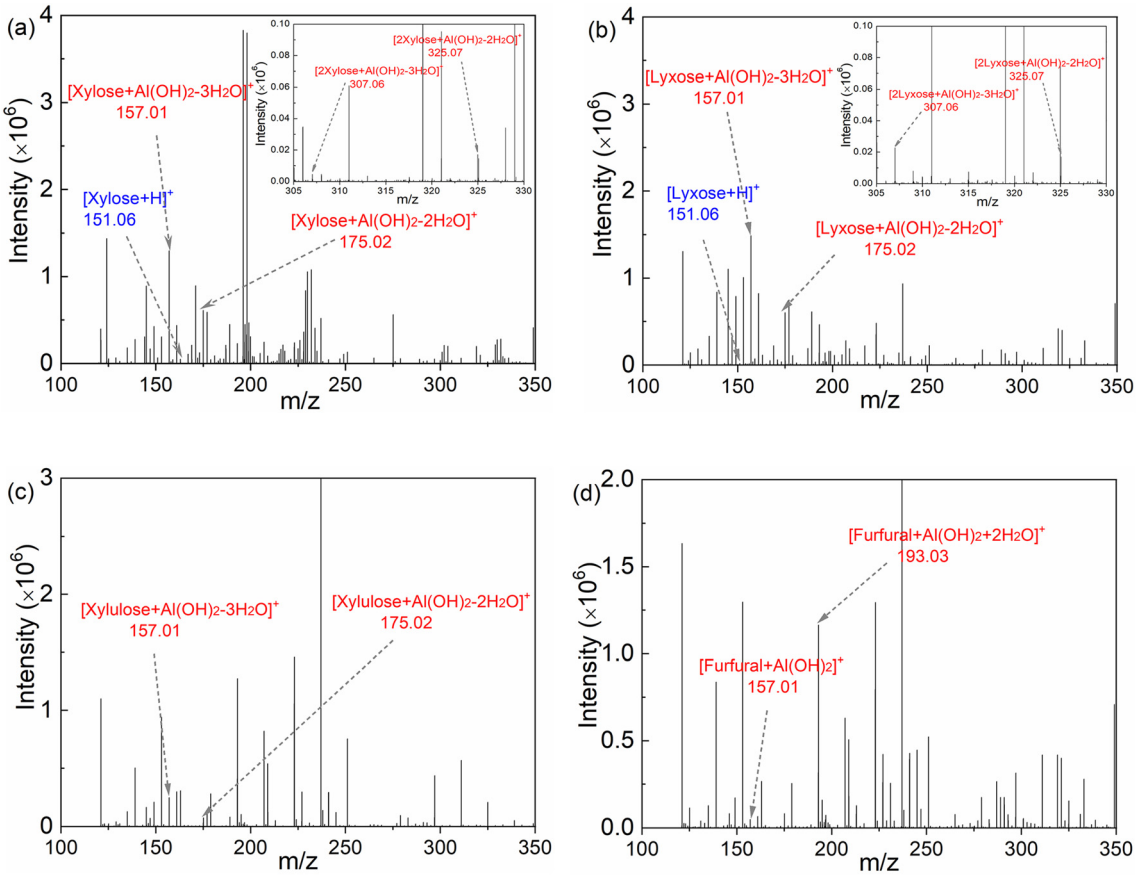

Fig. 5 ESI-MS spectra of the aqueous solution of 200 mM HCl and 40 mM $AlCl_3$ containing (a) 0.1 M xylose; (b) 0.1 M lyxose; (c) 0.1 M xylulose; and (d) 0.1 M furfural. Insets in (a) and (b) show a magnified view of the m/z region at 305–330.

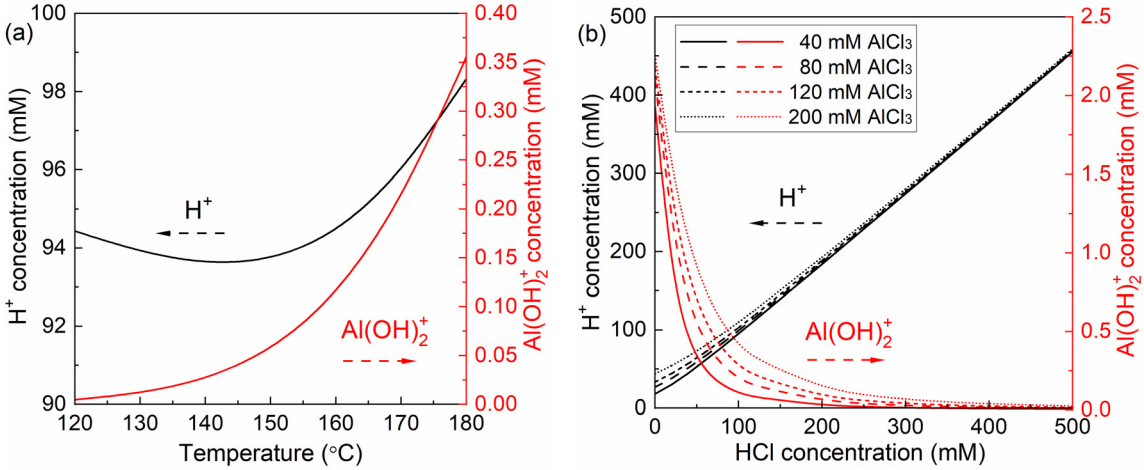

Fig. 6 Concentration of $Al(OH)_2^+$ and H^+ in water as a function of (a) temperature and (b) HCl concentration at different $AlCl_3$ concentrations. Conditions: 160 °C, 40 mM $AlCl_3$, 100 mM HCl (unless otherwise stated); concentrations are estimated according to eqn (S5)–(S8).†

increase of temperature and $AlCl_3$ concentration promotes the hydrolysis of $AlCl_3$ towards producing more H^+ and $Al(OH)_2^+$ (Fig. 6a and b; the slight decrease of H^+ concentration from 120 to 140 °C is caused by the volume increase of water at higher temperatures), while the increase of HCl concentration largely suppresses the formation of $Al(OH)_2^+$ (Fig. 6b). Such an interaction between $AlCl_3$ and HCl clearly indicates the importance of optimizing the relative Lewis/Brønsted acidity for the maximized furfural yields.

3.4 Kinetic behavior of the conversion of xylose, lyxose, xylulose and furfural in the microreactor

To acquire kinetic insights into xylose conversion over $AlCl_3$/HCl in water, monophasic experiments were conducted in microreactors regarding the effect of the reaction temperature and concentrations of substrate and catalyst (individual HCl, $AlCl_3$ or their combination) on the conversion of xylose, lyxose, xylulose and furfural in water. Moreover, biphasic experiments with varying O/A ratios and temperatures were also performed in microreactors to study the effect of the biphasic operation on the xylose conversion.

3.4.1 Monophasic experiments: effect of temperature and concentrations of acid catalyst and substrate. In the presence of HCl (200 mM), a higher temperature promotes both the conversion of sugars (and furfural) and the corresponding furfural yields (*cf.* Fig. 7a, b, and S4†), indicating the higher activation energy for the desirable sugar (xylose, lyxose and xylulose) dehydration reactions forming furfural than for furfural-involved side reactions over HCl. Comparatively, sugar conversions under the catalysis of $AlCl_3$ (40 mM) show somewhat different trends. That is, with increasing temperature, all substrate (xylose, lyxose, xylulose or furfural) conversion increased whereas the maximum yield of furfural as well as intermediate sugars (isomerization products) became lower at temperatures above *ca.* 160 °C (Fig. 7c, d and S5–S8†). Possible reasons could be a higher activation energy for the $Al(OH)_2^+$-catalyzed side reactions than for furfural formation, as well as an overall higher activation energy for the consumption of these isomerization products (to furfural or humins) than for their formation. Nevertheless, it was noticed that the amount of $Al(OH)_2^+$ and H^+ largely increased with increasing temperature (Table S5, entries 1–4†); *e.g.*, the $Al(OH)_2^+$ concentration in 40 mM $AlCl_3$ solution was estimated to increase from 0.72 mM at 120 °C to 2.72 mM at 180 °C (and from 7.1 to 25.6 mM for H^+), which might also have a significant impact on the product yields if the reaction orders in catalyst concentration for the sub-reactions are different. Thus, a comprehensive kinetic model should capture the temperature-dependency of both the sub-reactions of xylose conversion and the formation of $Al(OH)_2^+$ and H^+ in water quantitatively (*vide infra*).

For the HCl-catalyzed reactions of xylose, lyxose, xylulose and furfural in water, a higher HCl concentration significantly promoted their consumption rate, whereas a minor effect was observed on the maximum furfural yields from the sugars (Fig. S9†), which suggests similar reaction orders in H^+ concentration among the HCl-catalyzed sub-reactions. For the $AlCl_3$-catalyzed reactions, a very slight increase in sugar (xylose, lyxose and xylulose) conversion and a decrease in furfural yield were observed at higher $AlCl_3$ concentrations within the studied range (40–120 mM; Fig. S10–S13†), indicating an overall smaller reaction order in $Al(OH)_2^+$ for the desirable reaction forming furfural than for side reactions involving furfural within the $AlCl_3$-catalyzed sugar conversion network. Moreover, it was noticed that the actual concentration of the produced $Al(OH)_2^+$ did not differ much between these different initial $AlCl_3$ concentrations without the external HCl addition (being 1.93, 2.10 and 2.18 mM for 40, 80 and 120 mM $AlCl_3$, respectively; *cf.* Fig. 6b, entries 3, 5 and 6 of Table S5†), which explains the performance similarity in the sugar conversion among these varying $AlCl_3$ concentrations.

As revealed in Fig. 6b, a relatively larger difference in the amount of $Al(OH)_2^+$ between different initial $AlCl_3$ concen-

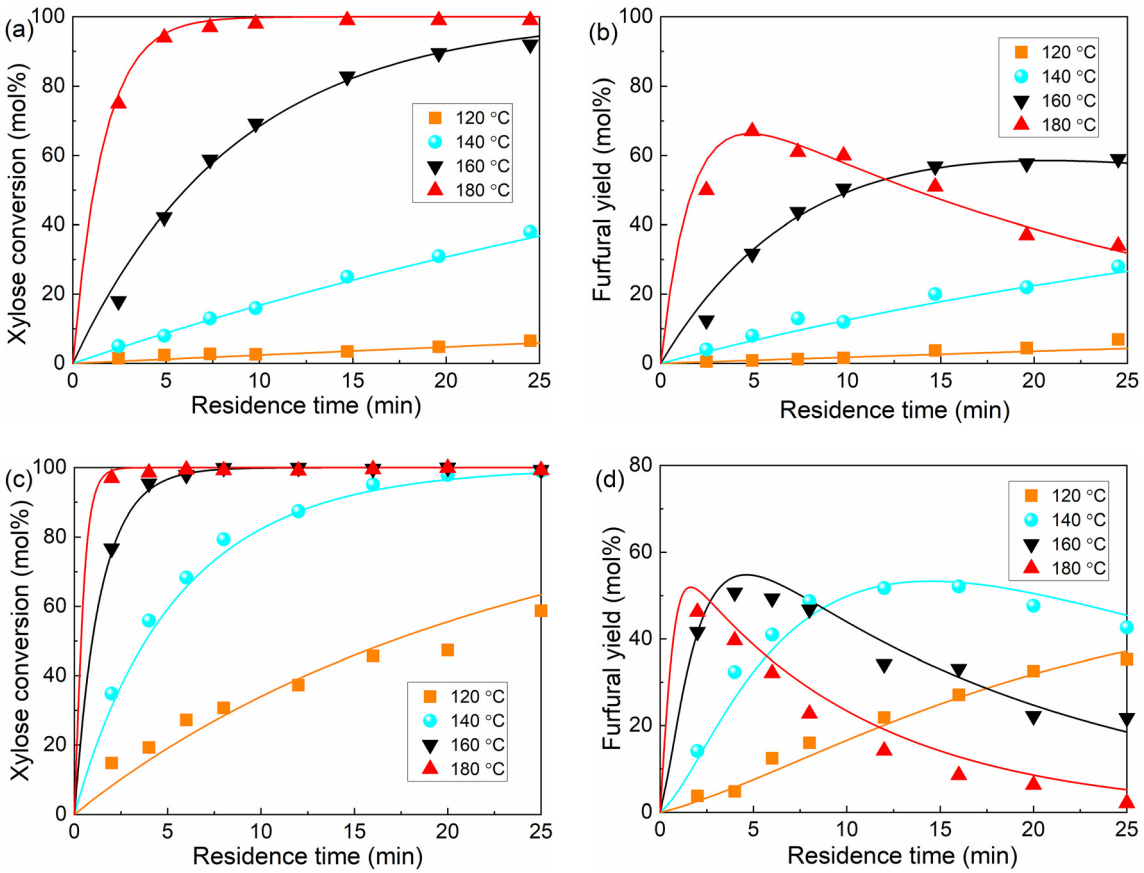

Fig. 7 Effect of temperature on xylose conversion in monophasic water in the microreactor. (a) Xylose conversion and (b) furfural yield over HCl; (c) xylose conversion and (d) furfural yield over $AlCl_3$. Reaction conditions: L = 3.3 m, 0.2 M HCl or 0.04 M $AlCl_3$, 0.1 M xylose.

trations can be realized with a proper addition of HCl (20–200 mM). Thus, $AlCl_3$ was used in combination with HCl (100 mM) to better study the effect of $Al(OH)_2^+$ concentration as well as the synergy between Lewis and Brønsted acids on the xylose conversion. It was observed that although the xylose conversion over combined $AlCl_3$/HCl is slower than in the $AlCl_3$-only case, it is still much faster compared with the HCl-only case, and increased monotonically with increasing $AlCl_3$ concentration (Fig. 8a). Considering the much smaller amount of $Al(OH)_2^+$ (in the $AlCl_3$-catalyzed case) than that of H^+ (in the

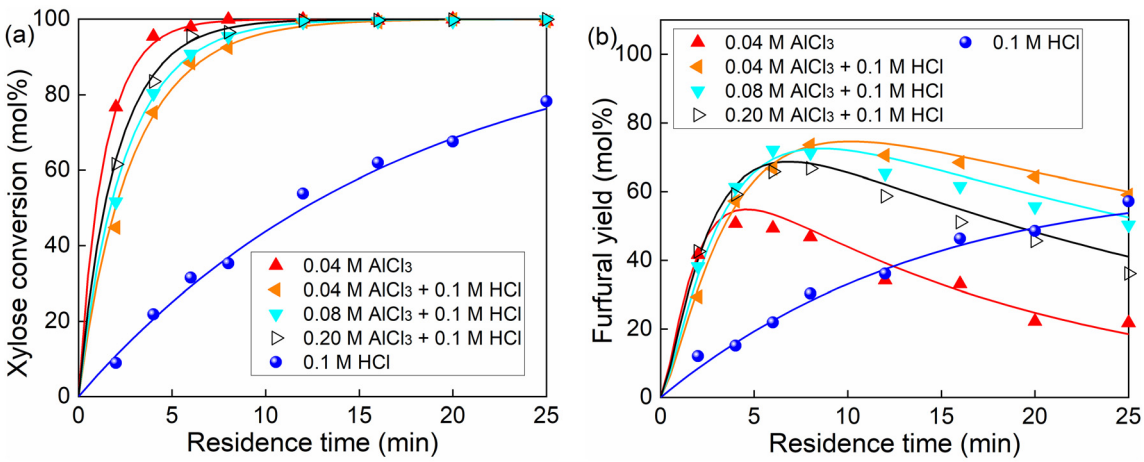

Fig. 8 Effect of the $AlCl_3$/HCl molar ratio on (a) xylose conversion and (b) furfural yields in water in the microreactor. Reaction conditions: 160 °C, 0.1 M xylose. The yields of lyxose and xylulose are given in Fig. S16.†

HCl-catalyzed case), the faster xylose conversion in the former case indicates a significantly higher activity of $Al(OH)_2^+$ than H^+. The higher concentration of $AlCl_3$ (and thus $Al(OH)_2^+$) promoted both the formation and consumption of the intermediate sugars, leading to their higher yields in the beginning but lower yields at later stage of the reaction (Fig. S16b and c†), which suggests lower reaction orders in $Al(OH)_2^+$ for the xylose isomerization reactions than for the further conversion of these isomers (to furfural or humins). Moreover, a relatively lower maximum furfural yield was obtained over $AlCl_3$ (40 mM) than over HCl (100 mM), due to the more severe side reaction over $Al(OH)_2^+$ leading to humins (Fig. 8b). Comparatively, the combined $AlCl_3$/HCl catalyst gave higher furfural yields than both $AlCl_3$ and HCl (Fig. 8b), though the furfural yield decreased with increasing $AlCl_3$ (or $Al(OH)_2^+$) concentration within the studied range (40–200 mM). This trend is in line with the xylose conversion over an $AlCl_3$-only catalyst of different amounts (Fig. S10d†). Thus, side reactions are believed to be of a higher reaction order in $Al(OH)_2^+$ than reactions forming furfural within the studied $AlCl_3$ concentration range.

For both HCl-catalyzed and $AlCl_3$-catalyzed cases, the reaction of xylose, lyxose, xylulose or furfural at different substrate concentrations shows a similar conversion of sugars (as well as the corresponding furfural yield) and conversion of furfural with the catalyst concentration (Fig. S14–S16†), which is indicative of an overall first-order reaction order with respect to the substrate (especially regarding the furfural formation) for both catalysts.

3.4.2 Biphasic experiments: effect of O/A ratios and temperature. To improve the furfural yield, xylose conversion experiments were performed in biphasic water–MIBK solvent systems (with 40 mM $AlCl_3$ and 100 mM HCl). Generally, a distinct improvement of the maximum furfural yield was realized by the biphasic operation (Fig. 9a), due to the furfural extraction into the organic phase leading to less furfural degradation in water. For example, the maximum furfural yield was increased from *ca.* 74% in monophasic water (at 160 °C in 12 min), to *ca.* 90% in the water–MIBK system (O/A = 4) (Fig. 9). Moreover, the promoting effect of increasing O/A ratio on the furfural yields quickly reached saturation as similar furfural yields were obtained at O/A ratios above 1. This indicates that the driving force and capacity for furfural extraction is sufficient even at a relatively low O/A ratio of 1, due to the high partition coefficient of furfural in MIBK being *ca.* 8 at 160 °C (eqn (31)). Moreover, the furfural yields also tend to be more stable in a biphasic system at prolonged residence times compared with monophasic water, though furfural in the organic phase is expected to be extracted back to water given a much longer reaction time, and to undergo further side reactions leading to a yield decrease. Furthermore, the effect of temperature on furfural yields in biphasic system was studied at an O/A of 4 (Fig. 9b). Similar to the results in monophasic water (Fig. 7b), the maximum furfural yields became lower at higher temperatures than 160 °C (Fig. 9b). In the biphasic system, temperature increase also promotes the phase partial miscibility leading to a more significant decrease in aqueous phase volume and thus an increase of two orders of magnitude in the $Al(OH)_2^+$ concentration (*e.g.*, 0.0042 mM at 120 °C to 0.3076 mM at 180 °C; Table S5, entries 14, 16–18†). Moreover, a higher temperature also leads to a lower furfural partition in MIBK (*cf.* eqn (31)). Therefore, the decrease of furfural yields at higher temperatures is an integrated result of these effects as well as the intrinsic kinetic properties of the sub-reactions, corroborating the importance of temperature selection and the development of a kinetic model for precise process analysis and optimization.

3.5 Kinetic modelling studies

The experimental studies in section 3.4 have shown a different temperature-dependency of xylose conversion over $AlCl_3$ and HCl, a different activity of $AlCl_3$ and HCl, as well as a positive effect of their combination for xylose conversion to furfural. For a comprehensive process understanding and optimization,

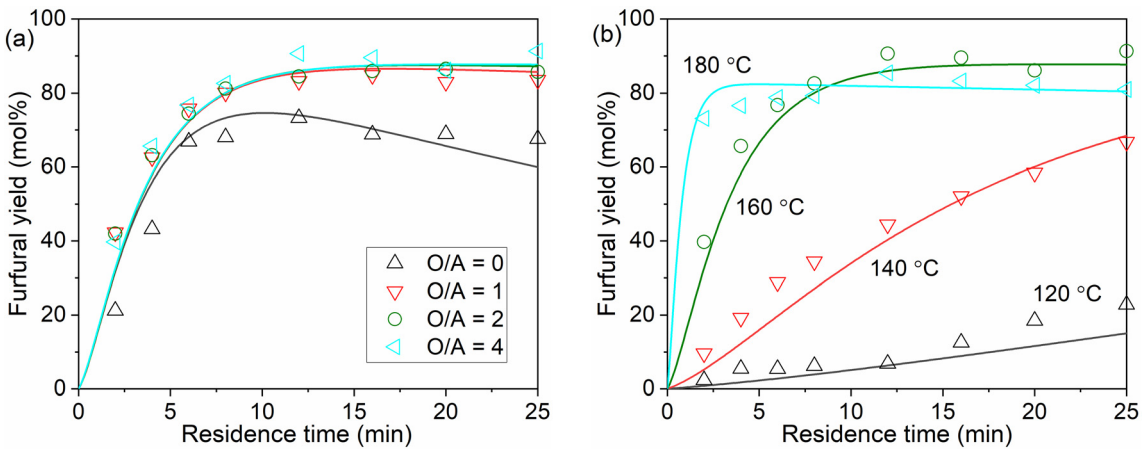

Fig. 9 Effect of (a) O/A ratios and (b) temperature on the furfural yield from xylose in the biphasic system. Reaction conditions: 160 °C (for a), 0.1 M xylose, 40 mM $AlCl_3$ and 100 mM HCl, O/A at 4 (for b).

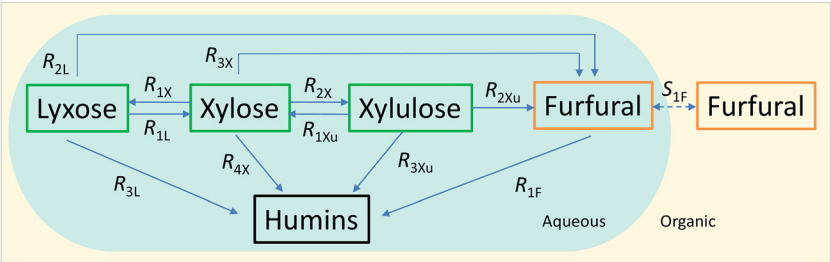

Fig. 10 Simplified overview of the xylose conversion network in the monophasic (water) and biphasic (water/MIBK) systems. An additional mass transfer of furfural between the two phases is present in the biphasic system. Label meanings are explained in the text.

a kinetic model that quantitatively captures the role of both Lewis and Brønsted acids ($Al(OH)_2^+$ and H^+) in xylose conversion and incorporates the furfural extraction between the phases is addressed herein.

In this section, the kinetic model for reactions in monophasic (water) and biphasic (water/MIBK) systems was established based on a simplified overview of the revealed xylose conversion network (*cf.* Fig. 4 and 10). In Fig. 10, R_{1X}, R_{2X}, R_{3X} and R_{4X} represent the reaction rates for xylose conversion to lyxose, xylulose, furfural and humins, respectively; R_{1L}, R_{2L} and R_{3L} are the reaction rates for lyxose conversion to xylose, furfural and humins, respectively; R_{1Xu}, R_{2Xu} and R_{3Xu} denote the reaction rates for xylulose conversion to xylose, furfural and humins, respectively; R_{1F} is the reaction rate for furfural degradation; and S_{1F} is the transfer rate of furfural from water to MIBK phase.

3.5.1 Kinetic model in the monophasic water system. The kinetic model was developed based on the results of reactions in monophasic water in microreactors using individual xylose, lyxose, xylulose and furfural as the starting substrate over HCl or (and) $AlCl_3$ as the catalyst, in which the substrate conversion and product yields were demonstrated as a function of the reaction temperature, residence time, and concentrations of acid catalyst and substrates (*cf.* Table S1† and Fig. 3, 7, 8, S4–S15†). Thus, the dependencies of the reaction rates on the temperature and concentrations are all captured by the kinetic model.

In the present monophasic microreactor system, it has been proved that the axial diffusion is negligible (characterized by the sufficiently large Bodenstein numbers of xylose and furfural of the order of *ca.* 10^6–10^7), and the parabolic velocity profile within the laminar flow can be compensated by the fast radial diffusion (characterized by the Fourier numbers of xylose and furfural being (much) larger than 1) to afford an approximate plug flow behaviour.[29,41] Therefore, here a simplified plug flow model was adopted for kinetic modelling.

Based on the reaction network in Fig. 10, the mole balance of different substances in water in microreactor can be expressed as

$$\frac{dC_{aq,xylose}}{d\tau} = -R_{1X} - R_{2X} - R_{3X} - R_{4X} + R_{1Xu} + R_{1L} \quad (6)$$

$$\frac{dC_{aq,lyxose}}{d\tau} = -R_{1L} - R_{2L} - R_{3L} + R_{1X} \quad (7)$$

$$\frac{dC_{aq,xylulose}}{d\tau} = -R_{1Xu} - R_{2Xu} - R_{3Xu} + R_{2X} \quad (8)$$

$$\frac{dC_{aq,furfural}}{d\tau} = -R_{1F} + R_{3X} + R_{2L} + R_{2Xu}. \quad (9)$$

In the present work, experimental studies regarding the effect of substrate concentration show that the sugar conversions (and the corresponding furfural yield) and the furfural conversion over either $AlCl_3$ or HCl are independent of the substrate concentrations (Fig. S14 and S15†). Therefore, a first-order dependence on the reactant is assumed for all H^+-catalyzed and $Al(OH)_2^+$-catalyzed sub-reactions. According to the role of Lewis and Brønsted acids in the xylose conversion network (Fig. 4), the rates of the sub-reactions (R_{ij}; i = 1, 2, 3 or 4; j = X, L, Xu or F, representing xylose, lyxose, xylulose or furfural, respectively, the same hereafter) can be divided into two groups: the ones catalyzed by only Lewis acids and the other ones catalyzed by both Lewis and Brønsted acids.

For reactions catalyzed by only Lewis acids (*i.e.*, R_{1X}, R_{2X}, R_{1L} and R_{1Xu}; Fig. 4 and 10), the reaction rates are defined as

$$R_{iX} = k_{L,iX}^{app} C_{aq,xylose} \quad (10)$$

$$R_{iL} = k_{L,iL}^{app} C_{aq,lyxose} \quad (11)$$

$$R_{iXu} = k_{L,iXu}^{app} C_{aq,xylulose} \quad (12)$$

and the rates of reactions catalyzed by both Lewis and Brønsted acid catalysts (*i.e.*, R_{3X}, R_{4X}, R_{2L}, R_{3L}, R_{2Xu}, R_{3Xu} and R_{1F}; Fig. 4, 8) are defined as

$$R_{iX} = (k_{L,iX}^{app} + k_{B,iX}^{app}) C_{aq,xylose} \quad (13)$$

$$R_{iL} = (k_{L,iL}^{app} + k_{B,iL}^{app}) C_{aq,lyxose} \quad (14)$$

$$R_{iXu} = (k_{L,iXu}^{app} + k_{B,iXu}^{app}) C_{aq,xylulose} \quad (15)$$

$$R_{iF} = (k_{L,iF}^{app} + k_{B,iF}^{app}) C_{aq,furfural} \quad (16)$$

In the above eqn (10)–(16), $k_{L,iX}^{app}$ and $k_{B,iX}^{app}$ (i = 1, 2, 3 or 4; j = X, L, Xu or F) are the apparent reaction rate constants for the sub-reactions catalyzed by a Lewis acid $Al(OH)_2^+$ and Brønsted acid H^+, respectively (*cf.* the more detailed definition in Table S6†). Considering the reversible epimerization between xylose and lyxose, and the isomerization between xylose and

xylulose, there are $k_{L,1L}^{app} = k_{L,1X}^{app}/K_{1X}$ and $k_{L,1Xu}^{app} = k_{L,2X}^{app}/K_{2X}$, where K_{1X} and K_{2X} are the corresponding equilibrium constants. The values of K_{1X} and K_{2X} under different temperatures are calculated from the kinetic parameters reported in the literature[42] and provided in Table S7.†

At the start of the reactions, the temperature of the reactant can be quickly raised from the initial room temperature (*ca.* 20 °C) to the final reaction temperature (T) within seconds due to the excellent heat transfer efficiency in the current microreactor setup;[19] as such this heating-up stage is reasonably neglected for kinetic modelling in this work. After heating-up, the density of the aqueous phase decreased so that its volumetric flow rate at the reaction temperature T (Q_{aq}) differed from its initial value at *ca.* 20 °C ($Q_{aq,0}$), and is corrected as

$$Q_{aq} = Q_{aq,0}\alpha_{mono,aq} \quad (17)$$

where $\alpha_{mono,aq}$ (ranging from 1.06 to 1.14 within 120–180 °C) is the ratio of the densities of the aqueous phase at 20 °C and T, and can be estimated as a function of T (in °C) from[29]

$$\alpha_{mono,aq} = 0.921 + 0.062e^{0.007T} \quad (18)$$

Considering the phase volume change, the conversion and yield in the model are calculated as

$$X_s = \frac{C_{aq,s,0} - \alpha_{mono,aq}C_{aq,s}}{C_{aq,s,0}} \times 100\% \quad (19)$$

$$Y_p = \frac{\alpha_{mono,aq}C_{aq,p}}{C_{aq,s,0}} \times 100\%. \quad (20)$$

In summary, the developed kinetic model for xylose conversion in monophasic water in microreactors comprises a set of nonlinear ordinary differential equations (ODE) for the mole balances of sugars and furfural (eqn (6)–(9)), together with equations to describe the reaction rates (eqn (10)–(16)) and phase volume change (eqn (17) and (18)). The apparent reaction rate constants ($k_{L,ij}^{app}$ and $k_{B,ij}^{app}$) were then determined by simultaneously processing the experimental data in Matlab R2010a (MathWorks) using the *lsqnonlin* nonlinear least-squares fitting function, based on a Trust-region-reflexive algorithm to perform a local minimization of the errors between the model values and experimental data (*i.e.*, in terms of the reactant conversion and product yields).

Considering the phase volume change, for a given set of initial concentrations of $AlCl_3$ and HCl at 20 °C (C_{AlCl_3}, 0 and $C_{HCl,0}$), there are $C_{AlCl_3} = C_{AlCl_3}$, $0/\alpha_{mono,aq}$ and $C_{HCl} = C_{HCl,0}/\alpha_{mono,aq}$ at the reaction temperature, which are needed for the estimation of $C_{Al(OH)_2^+}$ and C_{H^+} (*cf.* section S4 and Table S5†). For a first-order reaction with respect to the catalyst, the corresponding apparent reaction rate constant should be linearly dependent on the catalyst concentration. Such a linear relationship was clearly observed between $k_{B,ij}^{app}$ and C_{H^+} for all H^+-catalyzed sub-reactions (at 160 °C; Fig. S17a†), indicating a first-order for H^+ concentration. Thus, it is reasonable to describe $k_{B,ij}^{app}$ as

$$k_{B,ij}^{app} = k_{B,ij}C_{H^+} \quad (21)$$

Comparatively, a non-linear relationship was observed between $k_{L,ij}^{app}$ and $C_{Al(OH)_2^+}$ (*e.g.*, at 160 °C; not shown for brevity). Therefore, for $Al(OH)_2^+$-catalyzed sub-reactions a power law approach was applied with the reaction order in $Al(OH)_2^+$ as the unknown, and then $k_{L,ij}^{app}$ was described as

$$k_{L,ij}^{app} = k_{L,ij}C_{Al(OH)_2^+}{}^{nL,ij} \quad (22)$$

In eqn (21) and (22), $k_{B,ij}$ and $k_{L,ij}$ are the intrinsic reaction rate constants for H^+- and $Al(OH)_2^+$-catalyzed sub-reactions, respectively. $n_{L,ij}$ represents the reaction order in $Al(OH)_2^+$. Eqn (22) can be rearranged as

$$\ln k_{L,ij}^{app} = n_{L,ij} \ln C_{Al(OH)_2^+} + \ln k_{L,ij} \quad (23)$$

A linear relationship between $\ln k_{L,ij}^{app}$ and $\ln C_{Al(OH)_2^+}$ was obtained (Fig. S17b†), and after a linear regression, the corresponding reaction orders $n_{L,ij}$ and intrinsic reaction rate constants $k_{L,ij}$ were determined from the slopes and intercepts, respectively.

The temperature dependency of the intrinsic reaction rate constants ($k_{B,ij}$ or $k_{L,ij}$) is described according to the Arrhenius equation as

$$\ln k_{B,ij} = -\frac{Ea_{B,ij}}{RT} + \ln k_{0,B,ij} \quad \text{or}$$
$$\ln k_{L,ij} = -\frac{Ea_{L,ij}}{RT} + \ln k_{0,L,ij} \quad (24)$$

where $Ea_{B,ij}$ or $Ea_{L,ij}$ is the activation energy, and $k_{0,B,ij}$ or $k_{0,L,ij}$ is the pre-exponential factor, for the H^+- or $Al(OH)_2^+$-catalyzed sub-reactions, respectively. R is the gas constant (R = 8.3145 J mol^{-1} K^{-1}). The activation energy (Ea_{Bij} or $Ea_{L,ij}$) and pre-exponential factor ($k_{0,B,ij}$ or $k_{0,L,ij}$) for each sub-reaction were then estimated by plotting the natural logarithm of the intrinsic kinetic constant ($\ln k_{B,ij}$ or $\ln k_{L,ij}$) *versus* the inverse reaction temperature ($1/T$) and fitting according to the Arrhenius expression (eqn (24)). The best estimations of the intrinsic kinetic parameters and their standard deviations are given in Table 1. Generally, the H^+-catalyzed reactions have higher activation energies compared with the $Al(OH)_2^+$-catalyzed ones, in line with the observed higher activity of $Al(OH)_2^+$ than H^+ (Fig. 8). For H^+-catalyzed reactions, the activation energies for the desired sugar dehydration reaction producing furfural ($Ea_{B,3X}$, $Ea_{B,2L}$ and $Ea_{B,2Xu}$), and for the side reactions of sugar condensation to humins ($Ea_{B,4X}$, $Ea_{B,3L}$ and $Ea_{B,3Xu}$), are both higher than that for furfural degradation to humins. Similar results were also found in $Al(OH)_2^+$-catalyzed reactions, where activation energies for sugar condensation to humins ($Ea_{L,4X}$, $Ea_{L,3L}$, $Ea_{L,3Xu}$) are even higher than that for sugar dehydration to furfural ($Ea_{L,3X}$, $Ea_{L,2L}$, $Ea_{L,2Xu}$). This suggests that the formation of both furfural and humins from the sugars is promoted at higher temperatures, corroborating the importance of temperature analysis for maximized furfural yields (*vide infra*). Moreover, the reaction orders in $Al(OH)_2^+$ ($n_{L,ij}$) are smaller than 1, consistent with the higher activity of $Al(OH)_2^+$ than H^+ at a low amount, which was also revealed by the by far

Table 1 Estimated kinetic parameters for sub-reactions within the xylose conversion network over a Lewis acid $Al(OH)_2^+$ and Brønsted acid H^+ catalyst

		H^+		$[Al(OH)_2]^+$		
ij	Reaction	$\ln k_{0,B,ij}$ [b]	$Ea_{B,ij}$ (kJ mol^{-1})	$\ln k_{0,L,ij}$ [c]	$Ea_{L,ij}$ (kJ mol^{-1})	$n_{L,ij}$ [c]
1X	Xylose to lyxose[a]	—	—	26.4 ± 3.3	94.7 ± 11.4	0.28 ± 0.02
2X	Xylose to xylulose[a]	—	—	27.2 ± 1.7	97.3 ± 6.0	0.26 ± 0.02
3X	Xylose to furfural	38.1 ± 1.0	139.7 ± 4.4	15.0 ± 0.7	58.7 ± 2.4	0.25 ± 0.04
4X	Xylose to humins	34.6 ± 4.4	131.9 ± 6.3	31.5 ± 2.5	99.7 ± 8.7	0.95 ± 0.04
2L	Lyxose to furfural	45.2 ± 2.7	162.8 ± 18.2	24.8 ± 0.5	82.3 ± 1.8	0.19 ± 0.04
3L	Lyxose to humins	46.9 ± 2.4	171.1 ± 8.6	33.0 ± 0.7	99.4 ± 2.4	0.99 ± 0.03
2Xu	Xylulose to furfural	26.4 ± 0.0	94.2 ± 0.0	25.5 ± 2.4	88.7 ± 8.3	0.21 ± 0.03
3Xu	Xylulose to humins	23.2 ± 2.7	86.7 ± 8.9	32.4 ± 1.1	101.5 ± 3.7	0.98 ± 0.03
1F	Furfural to humins	21.2 ± 1.1	85.4 ± 5.1	8.1 ± 1.1	26.7 ± 4.0	0.56 ± 0.02

[a] Corresponding reversible reactions (R_{1L} and R_{1Xu}) were modeled using equilibrium constants calculated from the literature[42] (*cf.* Table S6†). [b] Units of k_0 expressed in L mol^{-1} min^{-1}. [c] Units of k_0 expressed in L$^{n_{L,ij}}$ mol$^{-n_{L,ij}}$ min^{-1}.

higher $k_{L,ij}^{app}$ than $k_{B,ij}^{app}$ at the same catalyst concentration within the studied range (Fig. S18a and b†). The reaction orders in $Al(OH)_2^+$ ($n_{L,ij}$) for sugar dehydration to furfural ($n_{L,3X}$, $n_{L,2L}$, $n_{L,2Xu}$) are also smaller than those for sugar condensation ($n_{L,4X}$, $n_{L,3L}$, $n_{L,3Xu}$) and furfural degradation to humins ($n_{L,1F}$), implying that humin formation from furfural and sugars is more enhanced at higher concentrations of $Al(OH)_2^+$ compared with furfural formation. This is consistent with the lower furfural yields over sole $AlCl_3$ than that catalyzed by combined $AlCl_3$/HCl (Fig. 8b); as such, the selection of acid concentration and a proper $AlCl_3$/HCl ratio is of importance in the process optimization (*vide infra*).

3.5.2 Kinetic model in the biphasic water/MIBK system. In the biphasic system, as a result of the partial miscibility between MIBK and water as well as the temperature dependency of the liquid density, the volumetric flow rate of both phases changed after mixing and fast heating from *ca.* 20 °C to the reaction temperature (T).[20] Therefore, for a given initial volumetric flow rate of two phases at 20 °C ($Q_{aq,0}$ or $Q_{org,0}$), their flow rates at the reaction temperature are corrected as[29]

$$Q_{aq,1} = Q_{aq,0}\alpha_{bi,aq} \quad (25)$$

$$Q_{org,1} = Q_{org,0}\alpha_{bi,org} \quad (26)$$

where $\alpha_{bi,aq}$ or $\alpha_{bi,org}$ is the correction factor that denotes the ratio of the flow rate after mixing at reaction temperature T to the initial flow rate at 20 °C (before mixing) for either the aqueous or the organic phase. For a given initial MIBK to water volumetric flow rate ratio (O/A) at 20 °C, α_{bi} is a function of T and estimated as[20]

$$\alpha_{bi} = u + ve^{wT} \quad (27)$$

where the values of the fitting parameters (u, v and w) are given in Table S3.†

It is assumed that the organic solvent MIBK is non-reactive and served only as an extraction medium;[20] then the mole balance in both phases ($C_{aq,furfural}$ and $C_{org,furfural}$) is described by

$$\frac{dC_{aq,furfural}}{d\tau} = -R_{1F} + R_{3X} + R_{2L} + R_{2Xu} - S_{1F} \quad (28)$$

$$\frac{dC_{org,furfural}}{d\tau} = \frac{Q_{aq}}{Q_{org}}S_{1F} \quad (29)$$

where S_{1F} is the extraction rate of furfural from the aqueous phase to the organic phase (Fig. 10), and is calculated as

$$S_{1F} = K_L a\left(C_{aq,furfural} - \frac{C_{org,furfural}}{m}\right) \quad (30)$$

where k_La is the mass transfer coefficient and m is the partition coefficient of furfural between MIBK and water. The value of m was measured (*cf.* details in section S10 and Fig. S19†) and estimated as a function of temperature by[29]

$$m = a - bT \quad (31)$$

where a = 10.137, b = 0.0154, and T is in °C.

In the current biphasic experiments in slug flow microreactors, the mass transfer limitation has been both theoretically estimated and experimentally proved to be absent (*cf.* section S11 and Fig. S21†); therefore the furfural concentrations in both phases can be also assumed to reach equilibrium immediately, as expressed by

$$C_{org,furfural} = mC_{aq,furfural} \quad (32)$$

By combining with eqn (29) and (32), eqn (28) is simplified to

$$\frac{dC_{aq,furfural}}{d\tau} = \frac{-R_{1F} + R_{3X} + R_{2L} + R_{2Xu}}{1 + m\dfrac{Q_{org}}{Q_{aq}}} \quad (33)$$

For given concentrations of HCl and $AlCl_3$ at 20 °C (*i.e.*, $C_{AlCl_3,0}$ and $C_{HCl,0}$), their concentrations at the reaction temperature in the biphasic system are corrected as $C_{AlCl_3} = C_{AlCl_3,0}/\alpha_{bi,aq}$ and $C_{HCl} = C_{HCl,0}/\alpha_{bi,aq}$, which are used for the estimation of $C_{Al(OH)_2^+}$ and C_{H^+} (*cf.* section S4 and Table S5†).

The model equations in the current biphasic system are represented by eqn (6)–(8) and (33) for the aqueous phase concentration and eqn (32) for the organic phase concentration. Based on the estimated kinetic constants (Table 1), the m values (eqn (31)) and the phase volume change (eqn (25)–(27)), the component concentration during the reaction was modelled. Then, substrate conversion (X_s) and product yield (Y_p) in the biphasic system in microreactor are calculated by

$$X_s = \frac{C_{aq,s,0} - \alpha_{bi,aq} C_{aq,s}}{C_{aq,s,0}} \times 100\% \quad (34)$$

$$Y_p = \frac{Q_{org} C_{org,p} + Q_{aq} C_{aq,p}}{Q_{aq,0} C_{aq,s,0}} \times 100\%. \quad (35)$$

3.5.3 Evaluation of the kinetic model. The predicting accuracy of the kinetic model was evaluated by comparing the model predictions with the experimental data *via* parity plots (Fig. S22†). The goodness of the fit was assessed by the coefficient of determination (R^2), calculated by

$$R^2 = 1 - \frac{\sum_{i=1}^{n} (x_i - \hat{x}_i)^2}{\sum_{i=1}^{n} (x_i - \bar{x}_i)^2} \quad (36)$$

where x_i is the experimental data (conversion or yield of the components), $\hat{x}_i$ is the predicted value by the kinetic model, $\bar{x}_i$ denotes the mean of the experimental data, and n indicates the number of experimental data.

For monophasic experiments, the developed kinetic model precisely predicts the evolution of the conversions or yields of all the components during the reaction in microreactors (Fig. 3, 7, 8, S4–S13†), and a good fit between the experimental data and model values was obtained for all components, as reflected in the corresponding R^2 being close to 1 (Fig. S22a†). In the biphasic system, though the experimental data thereof were not used for kinetic parameter estimation, still a good prediction of the evolution trend of the components (Fig. 2 and 9) as well as a good agreement between the experimental data and model predictions (Fig. S22b†) was achieved, supporting the validity of the current kinetic model.

3.6 Model implication and process optimization

3.6.1 Interaction between Lewis and Brønsted acids and its effect on xylose conversion. As elaborated in sections 3.2 and 3.3, both Lewis and Brønsted acids play a catalytic role in the xylose conversion network (Fig. 4), and Brønsted acidity regulates the hydrolysis of $AlCl_3$ and thus the amount of the catalytically active $Al(OH)_2^+$ species (Fig. 6b). Therefore, fine tuning of the concentration (ratios) of $AlCl_3$ and HCl is of importance for process optimization towards maximized furfural yields. The developed kinetic model enables the prediction of the maximum furfural yields in monophasic water under varying $AlCl_3$/HCl concentrations (*e.g.*, at 160 °C), and the corresponding time required to reach the maximum (Fig. 11). It is known that the increase of HCl addition leads to a sharp decrease in the amount of $Al(OH)_2^+$, which gradually levels off to a low value at high HCl concentrations (*e.g.*, <0.03 mM $Al(OH)_2^+$ obtained from 40 mM $AlCl_3$ with a high HCl concentration above 200 mM; *cf.* Fig. 6b). Accordingly, for all $AlCl_3$ concentrations, the maximum furfural yield firstly increases with increasing HCl addition and quickly reaches a maximum, due to the reduced $Al(OH)_2^+$-catalyzed humin formation. Subsequently, with a further increase of H^+ but decrease of $Al(OH)_2^+$, the maximum furfural yield decreases gradually from the peak, as H^+-catalyzed reactions (including that leading to humins) gradually become prevalent (Fig. 11a).

Generally, at a low HCl addition (0–20 mM), a minor difference in the maximum furfural yield was found between varying $AlCl_3$ concentrations within the studied range (Fig. 11), as also reflected in the experimental results of xylose conversion over 40, 80 and 120 mM $AlCl_3$ (Fig. S10†), which is because of the similar amount of $Al(OH)_2^+$ and H^+ therein (Fig. 6b). At a moderate HCl addition (*e.g.*, 20–200 mM), where a relatively large difference in the amount of $Al(OH)_2^+$ and H^+ was realized, a higher $AlCl_3$ addition leads to a lower maximum furfural yield, due to the higher reaction orders in

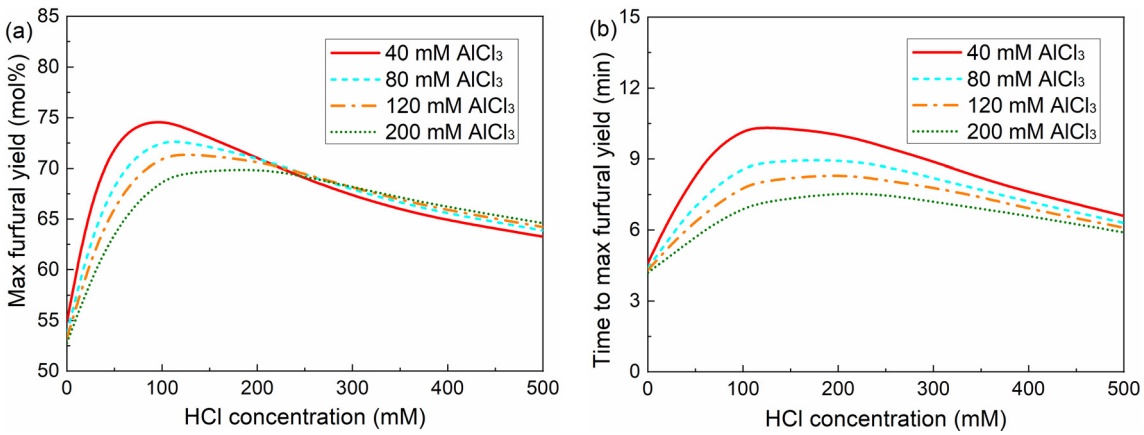

Fig. 11 (a) Maximum furfural yield and (b) time to reach the maximum furfural yield as a function of HCl concentration at different $AlCl_3$ concentrations. Other conditions: 160 °C, 0.5 M xylose, monophasic water.

$Al(OH)_2^+$ for reactions leading to humins than that for reactions producing furfural (Table 1). At a high HCl concentration over 200 mM, the difference in the maximum furfural yield among different $AlCl_3$ additions becomes minor again (a slightly lower furfural yield at lower $AlCl_3$ loading), as the hydrolysis of $AlCl_3$ is highly suppressed by high Brønsted acidity leading to a small amount of $Al(OH)_2^+$ generated, and as such xylose conversion tends to be catalyzed mainly by H^+. This is also consistent with the experimental findings that a minor difference in xylose conversion and furfural yield was observed for different $AlCl_3$ additions in combination with 200 mM HCl (Fig. 2). Moreover, a generally higher $AlCl_3$ concentration promotes the overall reaction rate (less time is required to reach the maximum furfural yield; Fig. 11b). Regardless of the $AlCl_3$ addition, with increasing HCl addition the overall reaction rate firstly decreases as the prevalent $Al(OH)_2^+$-catalyzed reactions are gradually suppressed, and then increases when H^+-catalyzed reactions are promoted and turn prevalent. Above all, the cooperativity between the $AlCl_3$ and HCl is dependent on the relative amount of the catalytically active $Al(OH)_2^+$ and H^+ therein, which affords different activity and selectivity for xylose conversion to furfural. Generally, the implications here are also well consistent with the experimental results reported in the literature on the C5/C6 sugar conversion to furfural or HMF over combined Lewis/Brønsted acid catalysts (*e.g.*, $CrCl_3$/HCl) in water.[30,31,43,44] Towards a maximized furfural yield and acceptable reaction rate, here 40 mM $AlCl_3$ and 100 mM HCl was selected as the optimized combination of Lewis and Brønsted acidity within the studied concentration range.

3.6.2 Effect of the biphasic operation: sensitivity analysis of extraction efficiency. As described in eqn (30), in the biphasic solvent system the furfural extraction rate is regulated by (i) the mass transfer coefficient (K_La), (ii) the partition coefficient (m), and (iii) the organic to aqueous volumetric flow ratio (O/A). Among others the inverse of the mass transfer coefficient ($1/K_La$) represents the extraction resistance, and both m and O/A influence the driving force and capacity for furfural extraction. Herein, a sensitivity analysis of these process parameters is performed to better understand their effect on furfural yields, using the kinetics under the optimal conditions of 40 mM $AlCl_3$ and 100 mM HCl at 160 °C (Fig. 12).

Generally, at a sufficient O/A of 4 and m of 8 (the partition coefficient of furfural in water/MIBK at 160 °C; eqn (31)), the furfural yield increases rapidly with the increase of K_La (*i.e.*, decrease of mass transfer resistance), and levels off after K_La reaches 0.5 min^{-1} (Fig. 12a). The plateau at K_La above 5 min^{-1} is due to the by far higher rate of furfural extraction than fur-

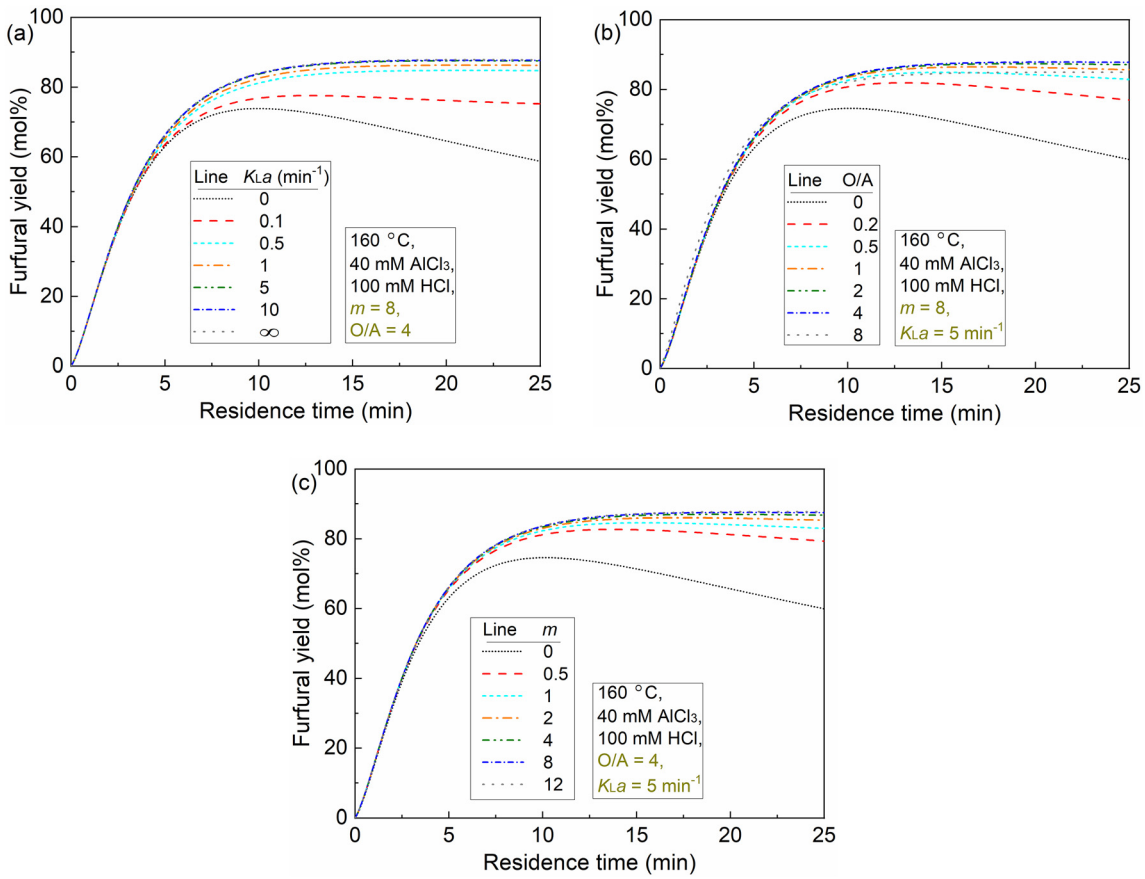

Fig. 12 Sensitivity analysis of extraction efficiency: effect of the (a) mass transfer coefficient; (b) organic to aqueous volumetric flow ratio; and (c) partition coefficient on furfural yields. Conditions: 160 °C, 0.5 M xylose, 40 mM $AlCl_3$ and 120 mM HCl.

fural degradation, indicating an absence of the mass transfer limitation. In principle, increases of both O/A and m lead to a higher driving force and capacity for furfural extraction. Under a high K_La of 5 min^{-1} and a high m (*e.g.* m = 8), the furfural yield increases fast with increasing O/A and reaches a plateau even at a low O/A ratio (*e.g.*, O/A = 0.5; Fig. 12b). Notably, a too high O/A ratio such as 8 might decrease the furfural yield due to the large phase volume change causing the $AlCl_3$/HCl concentration (ratio) to deviate from the optimal value (Fig. 12b and Table S5, entries 11–15†). Similarly, the analysis of m combined with high K_La (5 min^{-1}) and O/A (4) indicates that furfural yield increases with increasing m and quickly levels off even at a relatively low m of 2 (Fig. 12c). The analysis of O/A and m suggests their complementary relationship and similar promoting effect on the driving force and capacity for furfural extraction.

In our biphasic experiments in slug flow microreactors (L = 3.3 m), the K_La value is estimated to be sufficiently high (*e.g.*, being 2.5–8.9 min^{-1} for an O/A of 4, and should be even higher for lower O/A ratios given the higher interfacial area therein; *cf.* section S11). Considering also the high partition coefficient (m) of furfural in the water–MIBK system (being *ca.* 7–8 at 120–180 °C; *cf.* eqn (31)), our case is exactly the one shown in Fig. 12b, where the furfural yield should increase fast with the increase of O/A and reach a plateau even at a relatively low O/A level. This is correctly reflected in our experimental results regarding the effect of O/A ratios (Fig. 9), where the furfural yield was largely promoted even at a low O/A ratio of 1 while further increasing the O/A ratio only led to a slight further increase in the furfural yield. Considering also the cost of the organic solvent and its downstream separation, an initial O/A ratio of 4 was selected as the optimal for furfural synthesis.

3.6.3 Effect of temperature on xylose conversion in the monophasic and biphasic systems. Temperature plays a vital role in regulating the kinetic behavior of xylose conversion over combined $AlCl_3$ and HCl as the catalyst in a monophasic or biphasic system. Firstly, it regulates the kinetics of the different sub-reactions. The effect of temperature (within 120–180 °C) on sugar conversion and product yields over the individual Brønsted acid H^+ (120 mM) or Lewis acid $Al(OH)_2^+$ (0.1 mM) in monophasic water is studied based on the kinetic model, as shown in Fig. S23–S26.† Generally, an increase of temperature significantly promotes the conversion rates of the sugars. In the presence of H^+, the increase of temperature leads to higher maximum furfural yields from xylose, lyxose and xylulose (Fig. S23†), due to the higher activation energies for sugar dehydration to furfural than for furfural degradation (Table 1). Under the catalysis of $Al(OH)_2^+$, a higher reaction temperature leads to higher yields of intermediate sugars (Fig. S24–26†), due to the relatively higher (or similar) activation energies for their isomerization or epimerization compared with that for the further conversion of these intermediate sugars to furfural (or humins; *cf.* Table 1). In addition, the maximum furfural yield from the sugars is enhanced at higher reaction temperatures. This is because the activation energies for sugar dehydration are higher than that for furfural degradation (Table 1). Moreover, for all $Al(OH)_2^+$-catalyzed sugar conversions, the activation energies for sugar condensation to humins are the highest (Table 1). As such, the maximum furfural yields from all the sugars level off at temperatures over 160 °C (Fig. S10 and S11†), as the sugar condensation to humins is also significantly promoted, and a gradual decline of the maximum furfural yield is expected after extrapolation to a higher temperature beyond 180 °C.

In the presence of combined $AlCl_3$ and HCl as the catalyst, a higher reaction temperature not only promotes the kinetics, but also tends to shift the hydrolysis equilibrium of $AlCl_3$ in water towards generating more H^+ and $Al(OH)_2^+$ (Fig. 6). In the biphasic system, the increase of temperature leads to lower furfural partition in the MIBK phase (Fig. S19†) and thus less capacity and a lower driving force for furfural extraction. Moreover, the temperature also regulates the liquid density and partial miscibility between the water and MIBK, leading to the volume change of the two phases (Table S2†) and furthermore the concentration change of the reactants and catalysts. Taking into account all the abovementioned effects of temperature, the furfural yield from xylose conversion in the monophasic and biphasic systems at varying reaction temperatures is modeled under the optimized conditions (40 mM $AlCl_3$, 100 mM HCl, O/A = 4), as shown in Fig. 13.

In monophasic water, the maximum furfural yields are generally similar for temperatures between 120 and 160 °C, and gradually decrease at higher temperatures than 160 °C (Fig. 13a). In the biphasic system, a more distinct decreasing trend of furfural yields with increasing reaction temperature is found (Fig. 13b). This evolution trend of furfural yields with temperature is apparently different from that catalyzed by individual H^+ or $Al(OH)_2^+$ in water, where a higher temperature leads to higher furfural yields (Fig. S23–S26†). In the current water–MIBK biphasic system, the partition coefficient of furfural (*ca.* 7–8) and the actual O/A ratios (*ca.* 5–6) at 120–180 °C have been revealed to be sufficient (Fig. 12b) and thus should have a very limited effect on furfural yields with varying temperatures. Therefore, the decreased furfural yields at higher temperatures should be a result of the decreased aqueous phase volume and significantly increased concentration of Al $(OH)_2^+$ and H^+ in water (Table S5†), leading to somewhat of a deviation of the $Al(OH)_2^+/H^+$ concentration ratio from the optimal value. Generally, considering also the longer residence time to reach the maximum furfural yield at lower temperatures, 160 °C was selected as the optimized temperature for xylose conversion in the biphasic system.

3.6.4 Analysis of humin sources. The analysis of the humin sources based on the kinetic model indicates an increased humin formation from both xylose condensation and furfural degradation during the reaction under the catalysis of 100 mM HCl in monophasic water (Fig. S27a†). After the addition of 40 mM $AlCl_3$, the HCl-catalyzed humin formation from xylose and furfural are both largely suppressed, leading to a significantly improved maximum furfural yield (*e.g.*, from 59% to 75% at 160 °C), in spite of the presence of $Al(OH)_2^+$-catalyzed

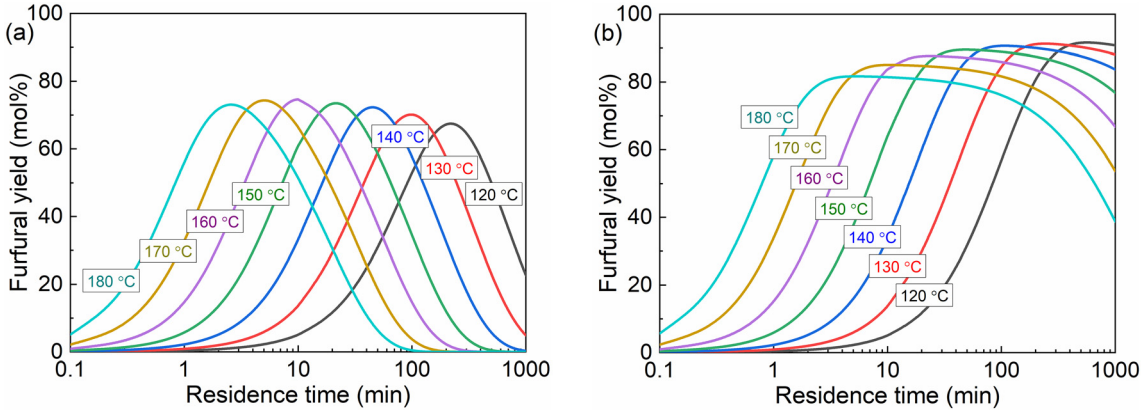

Fig. 13 Furfural yields from xylose at varying temperatures in the (a) monophasic water and (b) biphasic water–MIBK system. Conditions: 0.5 M xylose, 40 mM $AlCl_3$, 100 mM HCl, O/A = 4 (fed at 20 °C).

humin formation from xylose and furfural (Fig. S27a and b†). Furthermore, the modelling for the biphasic operation in slug flow microreactors (O/A = 4) proves the large elimination of both H^+- and $Al(OH)_2^+$-catalyzed humin formation from furfural degradation. As a result, the maximum furfural yield is further promoted from 75% to close to 90% (Fig. S27c†). Therefore, by a proper combination of HCl and $AlCl_3$ as well as the efficient furfural extraction in slug flow microreactors, the humin yield can be suppressed to a very large extent.

3.7 Optimized furfural synthesis in microreactors, catalyst recyclability and performance comparison with literature works

Based on the experimental results and model implications, favorable process conditions such as 160 °C, 40 mM $AlCl_3$, 100 mM HCl and O/A = 4 were adapted in combination with a high xylose concentration (*i.e.*, 1 M) to optimize the furfural (space–time) yields in slug flow microreactors. A highest furfural yield of up to 90% was achieved within a short residence time of 12 min at an almost full xylose conversion (Fig. 14a). The majority of furfural (*e.g.*, over 98% at 20 °C with O/A = 4) being extracted into the organic MIBK phase with a complete xylose conversion also largely facilitates the recycling of the catalytic aqueous phase by a simple phase separation (*via* decantation) followed by filtering out the small amount of humins. The recycled aqueous phase was then reused to prepare the fresh xylose feedstock for the following reaction runs. As shown in Fig. 14b, no distinct performance loss was observed after four consecutive 8-hour runs, corroborating the stability and sustainability of the present process. Additionally, the MIBK phase is also recyclable as it is feasible to separate furfural (boiling point: 162 °C at 101.3 kPa, and 90 °C at 8.7 kPa [45]) from MIBK (boiling point: 117 °C at 101.3 kPa, and 25 °C at 2.66 kPa [45]) by vacuum distillation at relatively lower temperatures (<80 °C) to avoid the thermal degradation of furfural which usually occurs at temperatures over 100 °C.[46]

The performance of the current catalytic and microreactor system was compared with the representative literature using homogeneous or heterogeneous catalysts for furfural synthesis from xylose in water–organic biphasic systems in batch or flow

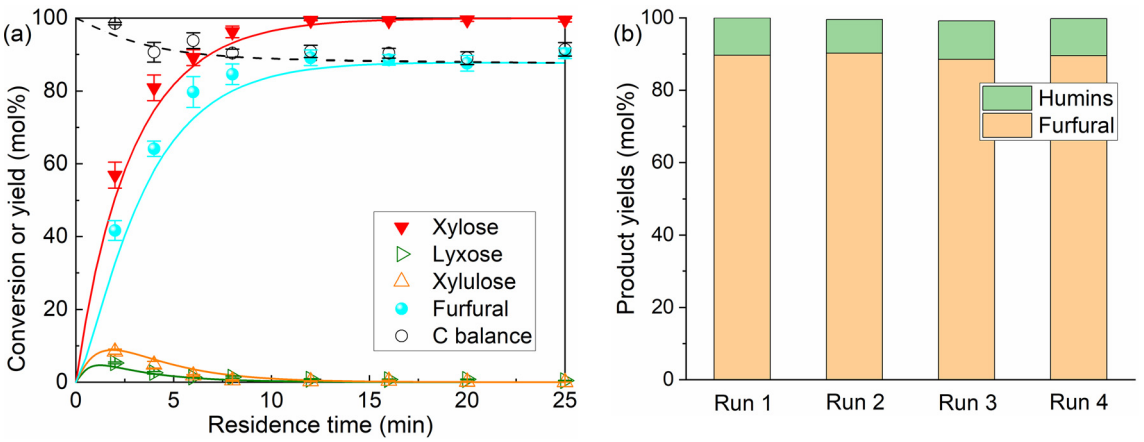

Fig. 14 (a) Optimized xylose conversion in slug flow microreactors; (b) reusability of the catalytic aqueous phase containing $AlCl_3$ and HCl (residence time 8 min and each run lasted for 8 hours). Reaction conditions: 160 °C, 1 M xylose, 40 mM $AlCl_3$, 100 mM HCl, O/A = 4 (fed at 20 °C).

reactors. Generally, in this work a much higher furfural yield (*e.g.*, $Y_{furfural}$ = 90%) and space–time yield (*e.g.*, $STY_{furfural}$ = 11.64 mol min^{-1} m^{-3}) were achieved from 1 M (15 wt%) xylose feedstock, compared with the literature using a batch reactor ($Y_{furfural}$ = 42–80%; $STY_{furfural}$ = 0.03–7.5 mol min^{-1} m^{-3}) (*cf.* details in Table S8†). The lower $STY_{furfural}$ in the literature is attributed to a lower substrate concentration, large reactor volume, and particularly the batch operation mode with an extended reaction time and limited furfural yields. In contrast, literature works related to the continuous flow reaction mode usually give a better $STY_{furfural}$. For example, Papaioannou *et al.*[47] conducted xylose conversion to furfural using H_2SO_4 as a catalyst in a water–toluene biphasic system in a slug flow millireactor (inner diameter: 4.1 mm). Despite the limited furfural yield (*ca.* 56%), still a good $STY_{furfural}$ was obtained (19.89 mol min^{-1} m^{-3}) thanks to a small reactor volume and a short residence time (2.5 min). In our previous work,[41] xylose conversion was performed over HCl/NaCl in a slug flow microreactor, where a meritorious furfural yield (93%) and $STY_{furfural}$ of 35.96 mol min^{-1} m^{-3} were achieved from 1 M xylose. However, it was found that the addition of 10 wt% NaCl (used as a promotor) in water largely increased the viscosity and thus the operation difficulty for the microreactor system. As such, the present catalytic system in this work holds its unique merits in addition to desirable furfural (space–time) yields (*e.g.*, mild operation requirements for the microreactor setup with only a low concentration of $AlCl_3$ as an additional catalyst component). Besides water, non-aqueous solvents have also been reported to be effective for xylose conversion, such as ionic liquids, polar aprotic solvents like DMSO, and deep eutectic solvents.[48–50] However, though good yields were obtained (over 60%), these systems are still in the early stage of lab-scale research and gave a relatively low $STY_{furfural}$ due to a long reaction time and batch reaction mode, not to mention the high cost and difficulty in downstream furfural separation. Therefore, this work using water as a cheap and green solvent, and $AlCl_3$/HCl as a low-cost, recyclable and low-toxicity catalyst, with the high furfural (space–time) yield achieved in a slug flow microreactor, represents a promising approach for efficient furfural synthesis.

4. Conclusion

Furfural production from lignocellulose-derived carbohydrates such as xylose represents an important reaction with a long history in bio-refineries. Experimental findings have been reported regarding the promoting effect of a Lewis acid (in combination with a Brønsted acid) on xylose conversion to furfural. In order to acquire deep insights into the reaction network and kinetics for better process understanding and optimization, we performed systematic experimental and kinetic modelling studies on xylose conversion, using $AlCl_3$/HCl as a combined Lewis/Brønsted acid catalyst in both monophasic water and biphasic water–MIBK systems, over a broad range of reaction conditions such as a temperature window of 120 to 180 °C, HCl concentrations of 0.05 to 0.4 M, $AlCl_3$ concentrations of 0.04 to 0.12 M, and initial substrate (xylose, lyxose, xylulose and furfural) concentrations of 0.01 to 0.5 M. Microreactors were used as both a platform for the fast monophasic kinetic experiments, and a process intensification tool for the efficient furfural synthesis in the biphasic system (under slug flow pattern). After optimization, a furfural yield up to 90% from 1 M xylose was achieved over 40 mM $AlCl_3$ and 100 mM HCl at 160 °C and 12 min.

Based on the experimental results, an extensive reaction network was revealed covering a series of parallel and tandem reactions of isomerization, dehydration and degradation from xylose. The regulatory role of the Lewis and Brønsted acids therein was interpreted as that only Lewis acid catalyzes the isomerization and epimerization between xylose, lyxose and xylulose, while both the Lewis and Brønsted acids are active for sugar dehydration to furfural and side reactions leading to humins such as sugar condensation and furfural degradation. Particularly, the promoting effect of Lewis acid on xylose conversion to furfural is attributed to not only the tandem catalysis *via* xylulose, but also the parallel direct Lewis acid-catalyzed sugar dehydration. Through ESI-MS spectroscopy characterization, $Al(OH)_2^+$ was identified as the active Al species that coordinates with xylose, furfural and intermediate sugars (lyxose and xylulose) in water, thus behaving as Lewis acid sites responsible for the sub-reactions within the xylose conversion network. The amount of $Al(OH)_2^+$ and H^+ in water was determined *via* the hydrolysis equilibrium of $AlCl_3$ given a certain temperature and initial concentration of $AlCl_3$ and HCl, and used for the development of the kinetic model from the results of the monophasic experiments. The model can also predict well the results of biphasic experiments after the incorporation of furfural extraction between the two phases, with the consideration of phase volume change as a function of temperature and phase partial miscibility. The rates of all sub-reactions behave with a first-order dependency on the substrates and H^+, while their reaction orders in $Al(OH)_2^+$ were estimated to fall in the range 0.19–0.99. Experimental results and model predictions revealed a volcano-like dependency of the achievable maximum furfural yields (in monophasic water) on the relative molar ratios of HCl to $AlCl_3$ (and furthermore, the molar ratio of $Al(OH)_2^+$ to H^+), whereas varying the concentration of HCl or $AlCl_3$ as a sole catalyst is not effective for improving furfural yields. This evolution trend of furfural yields with the increase of HCl/$AlCl_3$ molar ratio is related to (i) the lower reaction orders in $Al(OH)_2^+$ for the reactions producing furfural than that for side reactions; and (ii) a gradual shift of the dominant reaction from $Al(OH)_2^+$-catalyzed pathways towards H^+-catalyzed ones.

Model prediction assuming $Al(OH)_2^+$ or H^+ as the sole catalyst shows higher furfural yields with temperature increase within the studied range for both $Al(OH)_2^+$- and H^+-catalyzed reactions due to the higher activation energy for furfural formation reactions than that for furfural degradation. However, in the $AlCl_3$-involved reactions (containing both $Al(OH)_2^+$ and H^+) the experiments and model implication show similar (for

monophasic experiments) or lower (for biphasic experiments) furfural yields with the increase of temperature. This is due to the more promoted hydrolysis of $AlCl_3$ and significant phase volume change (particularly for the biphasic system with larger partial phase miscibility) at higher temperatures, leading to a deviation of the $Al(OH)_2^+/H^+$ molar ratio from the optimal value and thus lower furfural yields. In the present slug flow microreactor, the furfural extraction rate was estimated to be two orders of magnitude higher than the rate of furfural degradation, rendering the reaction under kinetic control, which has also been experimentally proved with varying microreactor lengths. An analysis of humin sources (*i.e.*, xylose condensation or furfural degradation) indicates that the former side reaction is largely suppressed by the improved chemistry from properly combined $AlCl_3$/HCl, and the latter is almost completely prevented in the biphasic system by the efficient furfural extraction and high furfural partition into MIBK. As a result, the furfural (space–time) yield in this work is rather promising compared with the literature. High furfural partition into the organic phase also allowed a simple downstream phase separation and recycling of the catalytic aqueous phase, which was used for four consecutive 8-hour runs without distinct performance loss.

Generally, this work revealed useful insights for understanding the complicated reaction network and kinetics of xylose conversion over combined Lewis/Brønsted acids, and demonstrated an efficient and sustainable process for furfural synthesis using slug flow microreactors as a production platform.

Conflicts of interest

The authors declare that there is no conflict of interest.

Acknowledgements

Part of the present research was financially supported by the University of Groningen (start-up package in the area of green chemistry and technology). The China Scholarship Council is gratefully acknowledged for financial support (grant number 201606740069 for Wenze Guo). Wenze Guo gratefully acknowledges Dr Jozef G. M. Winkelman for the insightful discussions on kinetic modelling details.

References

1 A. Corma, S. Iborra and A. Velty, *Chem. Rev.*, 2007, **107**, 2411–2502.
2 G. W. Huber, S. Iborra and A. Corma, *Chem. Rev.*, 2006, **106**, 4044–4098.
3 R.-J. van Putten, J. C. van der Waal, E. de Jong, C. B. Rasrendra, H. J. Heeres and J. G. de Vries, *Chem. Rev.*, 2013, **113**, 1499–1597.
4 L. T. Mika, E. Cséfalvay and Á. Németh, *Chem. Rev.*, 2018, **118**, 505–613.
5 P. Mäki-Arvela, T. Salmi, B. Holmbom, S. Willför and D. Y. Murzin, *Chem. Rev.*, 2011, **111**, 5638–5666.
6 R. Mariscal, P. Maireles-Torres, M. Ojeda, I. Sádaba and M. López Granados, *Energy Environ. Sci.*, 2016, **9**, 1144–1189.
7 J. A. Brydson, in *Plastics Materials (Seventh Edition)*, ed. J. A. Brydson, Butterworth-Heinemann, Oxford, 1999, pp. 810–813.
8 F. Dong, Y. Zhu, G. Ding, J. Cui, X. Li and Y. Li, *ChemSusChem*, 2015, **8**, 1534–1537.
9 J. Kijeński, P. Winiarek, T. Paryjczak, A. Lewicki and A. Mikołajska, *Appl. Catal., A*, 2002, **233**, 171–182.
10 D. F. Aycock, *Org. Process Res. Dev.*, 2007, **11**, 156–159.
11 G. W. Huber, J. N. Chheda, C. J. Barrett and J. A. Dumesic, *Science*, 2005, **308**, 1446.
12 B. Danon, G. Marcotullio and W. de Jong, *Green Chem.*, 2014, **16**, 39–54.
13 H. J. Brownlee and C. S. Miner, *Ind. Eng. Chem.*, 1948, **40**, 201–204.
14 R. Karinen, K. Vilonen and M. Niemelä, *ChemSusChem*, 2011, **4**, 1002–1016.
15 J. S. Kruger, V. Nikolakis and D. G. Vlachos, *Curr. Opin. Chem. Eng.*, 2012, **1**, 312–320.
16 R. Weingarten, G. A. Tompsett, W. C. Conner and G. W. Huber, *J. Catal.*, 2011, **279**, 174–182.
17 W. Guo, E. J. M. Hensen, W. Qi, H. J. Heeres and J. Yue, *ACS Sustainable Chem. Eng.*, 2022, **10**, 10157–10168.
18 W. Guo, T. Kortenbach, W. Qi, E. Hensen, H. Jan Heeres and J. Yue, *Appl. Catal., B*, 2022, **301**, 120800.
19 W. Guo, H. J. Heeres and J. Yue, *Chem. Eng. J.*, 2020, **381**, 122754.
20 W. Guo, Z. Zhang, J. Hacking, H. J. Heeres and J. Yue, *Chem. Eng. J.*, 2021, **409**, 128182.
21 R. M. Abdilla-Santes, W. Guo, P. C. A. Bruijnincx, J. Yue, P. J. Deuss and H. J. Heeres, *ChemSusChem*, 2019, **12**, 4304–4312.
22 M. Brasholz, K. von Kanel, C. H. Hornung, S. Saubern and J. Tsanaktsidis, *Green Chem.*, 2011, **13**, 1114–1117.
23 T. M. Kohl, B. Bizet, P. Kevan, C. Sellwood, J. Tsanaktsidis and C. H. Hornung, *React. Chem. Eng.*, 2017, **2**, 541–549.
24 T. Shimanouchi, Y. Kataoka, T. Tanifuji, Y. Kimura, S. Fujioka and K. Terasaka, *AIChE J.*, 2016, **62**, 2135–2143.
25 Y. Muranaka, H. Nakagawa, R. Masaki, T. Maki and K. Mae, *Ind. Eng. Chem. Res.*, 2017, **56**, 10998–11005.
26 P. Desir, B. Saha and D. G. Vlachos, *Energy Environ. Sci.*, 2019, **12**, 2463–2475.
27 J. A. Bennett, Z. S. Campbell and M. Abolhasani, *Curr. Opin. Chem. Eng.*, 2019, **26**, 9–19.
28 J.-i. Yoshida, H. Kim and A. Nagaki, *ChemSusChem*, 2011, **4**, 331–340.
29 W. Guo, H. C. Bruining, H. J. Heeres and J. Yue, *AIChE J.*, 2022, **68**, e17606.
30 V. Choudhary, S. I. Sandler and D. G. Vlachos, *ACS Catal.*, 2012, **2**, 2022–2028.

31 M. Lopes, K. Dussan and J. J. Leahy, *Chem. Eng. J.*, 2017, **323**, 278–286.
32 Y. Yang, C.-W. Hu and M. M. Abu-Omar, *ChemSusChem*, 2012, **5**, 405–410.
33 T. Yang, Y.-H. Zhou, S.-Z. Zhu, H. Pan and Y.-B. Huang, *ChemSusChem*, 2017, **10**, 4066–4079.
34 A. Mittal, H. M. Pilath and D. K. Johnson, *Energy Fuels*, 2020, **34**, 3284–3293.
35 J. Tang, L. Zhu, X. Fu, J. Dai, X. Guo and C. Hu, *ACS Catal.*, 2017, **7**, 256–266.
36 R. Noma, K. Nakajima, K. Kamata, M. Kitano, S. Hayashi and M. Hara, *J. Phys. Chem. C*, 2015, **119**, 17117–17125.
37 K. Nakajima, R. Noma, M. Kitano and M. Hara, *J. Mol. Catal. A: Chem.*, 2014, **388**, 100–105.
38 K. Nakajima, Y. Baba, R. Noma, M. Kitano, J. N. Kondo, S. Hayashi and M. Hara, *J. Am. Chem. Soc.*, 2011, **133**, 4224–4227.
39 K. Nakajima, R. Noma, M. Kitano and M. Hara, *J. Phys. Chem. C*, 2013, **117**, 16028–16033.
40 W. L. Bourcier, K. G. Knauss and K. J. Jackson, *Geochim. Cosmochim. Acta*, 1993, **57**, 747–762.
41 W. Guo, Doctoral dissertation, University of Groningen, 2021. DOI: **10.33612/diss.178033475**.
42 I. Delidovich, M. S. Gyngazova, N. Sánchez-Bastardo, J. P. Wohland, C. Hoppe and P. Drabo, *Green Chem.*, 2018, **20**, 724–734.
43 T. D. Swift, H. Nguyen, A. Anderko, V. Nikolakis and D. G. Vlachos, *Green Chem.*, 2015, **17**, 4725–4735.
44 V. Choudhary, A. B. Pinar, S. I. Sandler, D. G. Vlachos and R. F. Lobo, *ACS Catal.*, 2011, **1**, 1724–1728.
45 NIST Chemistry Webbook., **https://webbook.nist.gov/chemistry/fluid/**.
46 J. N. Chheda, Y. Román-Leshkov and J. A. Dumesic, *Green Chem.*, 2007, **9**, 342–350.
47 M. Papaioannou, R. J. T. Kleijwegt, J. van der Schaaf and M. F. Neira d'Angelo, *Ind. Eng. Chem. Res.*, 2019, **58**, 16106–16115.
48 E. Lam, E. Majid, A. C. W. Leung, J. H. Chong, K. A. Mahmoud and J. H. T. Luong, *ChemSusChem*, 2011, **4**, 535–541.
49 S. Peleteiro, S. Rivas, J. L. Alonso, V. Santos and J. C. Parajó, *Bioresour. Technol.*, 2016, **202**, 181–191.
50 E. S. Morais, M. G. Freire, C. S. R. Freire, J. A. P. Coutinho and A. J. D. Silvestre, *ChemSusChem*, 2020, **13**, 784–790.